2005

# Mechanical testing of vacuum infused specimens : sandwich interface strength and a braided sandwich connection

Drew Truxel
*Lehigh University*

Truxel, Drew

# Mechanical Testing of Vacuum Infused Specimens Sandwich Interface...

May 2005

# Mechanical Testing of Vacuum Infused Specimens

**Sandwich interface strength and a braided sandwich connection**

By

Drew Truxel

A Thesis

Presented to the Graduate and Research Committee

of Lehigh University

in Candidacy for the Degree of

Master of Science

in the

Department of Mechanical Engineering
and Mechanics

Lehigh University
May, 2005

This thesis is accepted and approved in partial fulfillment of the requirements for the Master of Science.

April 29, 2005
Date

Thesis Advisor

Chairperson of Department

## Acknowledgements

The research of this thesis was carried out between March 2004 and May 2005 in the Composites Lab within the Department of Mechanical Engineering and Mechanics at Lehigh University. I sincerely thank all of my fellow graduate students and professors and acknowledge their support. I especially wish to thank the following people:

Dr. Joachim L. Grenestedt who has served as my advisor during the course of my research. He has supported me in every way possible and has been an excellent teacher. His enthusiasm, work ethic, and sense of humor have inspired me to reach new levels and to question everything. I have learned that there are actually 30 hours in each day and to laugh every time I hear or think the word impossible.

Dr. Parsaroan Hutapea who helped proof read the majority of papers that I've written and is now a professor at Temple University.

Bill Maroun who is clearly 'the man'. He is extremely knowledgeable and hard working. He is always there to lend a hand, smooth over bad situations, and no matter how bad things are he always has the best attitude.

Jun Cao, Jack Reany, Eric Hahn and Chris Wonderly, my fellow graduate students working in the Composites Lab. I thank them all for their help, either lending an extra hand or helping me get through the 30 hour days.

Dick Towne, Bob Minnich, and Jim Bunderla for their help in keeping my projects in motion.

My friends and family who have given me their unending and unwavering support over the last 24 years. Without them I would not be where I am today.

Table of Contents

**Abstract** 1

**Introduction and Summary** 2

Appended papers

Paper A

"Influence of Face/Core Interface & Resin on Debond Toughness of Foam and Balsa Cored Sandwich" 7

Paper B

"Manufacturing and Testing of a Braided Pi Section" 43

**Vita** 59

## Thesis

This thesis comprises an introduction and the following two papers:

PAPER A:

Truxel, A., Aviles, F., Grenestedt, J.L., Carlsson, L.A., "Influence of Face/Core Interface and Resin on Debond Toughness of Foam and Balsa Cored Sandwich," 2005.

PAPER B:

Truxel, A., Grenestedt J.L., Maroun, B., "Manufacturing and Testing of a Braided Pi Section," 2004.

For my M.Sc. degree, I also wrote a third paper which is presently classified.

## Abstract

This thesis concerns two concepts of vacuum infused specimens that were manufactured and mechanically tested: the face/core interface strength of foam core sandwich specimens with differently manufactured interfaces, and a sandwich connection method using a three-dimensionally braided glass fiber.

In the first appended paper, the face/core interface was manufactured in five different ways for two different core materials. The Tilted Sandwich Debond (TSD) test was used to measure the debond fracture toughness. There was roughly a 50% increase in fracture toughness from the method producing the lowest to the method producing the highest fracture toughness. The foam cored specimens on average, produced approximately 60% higher fracture toughness than the balsa cored specimens. Regardless of core, using continuous filament mat between the core and fibers produced the highest fracture toughness.

The second appended paper describes the manufacturing and preliminary testing of a pi shaped three-dimensional braided glass fiber preform infused with epoxy. The specimens were vacuum infused around an aluminum mandrel. After cure, specimens were cut using a waterjet cutter. Two specimens were bonded to a flat plate and mechanically tested to failure. The second specimen produced a failure load three times higher than the first. The difference between the first and second specimens was the surface preparation before bonding, and the curing scheme.

## Introduction and Summary

This thesis concerns the face/core interface in composite sandwich structures and the manufacture of a glass fiber/epoxy braided 'pi shaped' section.

Presently there is a trend towards making stronger, more lightweight and more cost effective structures. These structures can be found in aerospace, navel, automotive and public transportation vehicles, bridges and other civil infrastructure, and sporting equipment. Composites are particularly well suited for aerospace and marine vehicles because of high strength and stiffness to weight ratios, high corrosion and fatigue resistances, and the ability to be manufactured into complex shapes.

Composite sandwich structures generally consist of a low density core between two high strength face sheets. The thicker the core, the further the skins are from the neutral axis, making the sandwich stronger and stiffer. The skins take the majority of the in-plane and bending loads, while the core takes shearing loads and prevents sandwich panels with thin skins from wrinkling. The strength of the sandwich is greatly dependent upon the face/core interface and how it was manufactured. If there is a poor bond between the core and the face sheets, then the sandwich's strength is reduced and the face sheets could debond. If a chain is only as strong as its weakest link, then a composite sandwich panel may be only as strong as its weakest face/core interface.

A major challenge is joining sandwich panels. A lot of time and effort has gone into researching efficient ways of joining a sandwich panel to another structure. These methods include for example bolting L shaped brackets to the sandwich panel and bulkhead, making a T joint with putty and composite, making an interface to bolt to. In

order to save time, money, weight, and increase strength, three dimensional braided structures are being studied as a means to join sandwich panels.

**Face/core Interface Manufacture**

The face/core interface of a composite sandwich panel is a very important part of the panel's integrity. The manner in which the interface was manufactured is also very important. The Diab Divinycell H-Grade and ProBalsa Technical Manuals [1, 2] advise vacuum cleaning and priming the cores prior to vacuum infusion. Using a vacuum cleaner instead of, for example, compressed air to reduce the risk of oil from the air line to contaminate the interface, would affect the adhesion. Priming the core with a coating of quick curing resin may reduce the risk that the core drains excessive amounts of resin from the skins and thus creates a resin starved interface. The author could not find a comparison of how different methods of resin infusion affect the face/core interface. However, there has been a lot of research done on modeling and testing the interface. Grenestedt introduced the Tilted Sandwich Debond (TSD) method of testing debond fracture toughness. This method was later studied in detail by Li et al. [5]. Majumdar, et. al. [3] studied the effects of temperature processing, suction, and foam density on the fracture toughness using the TSD test method. Li et al., [5] concluded that specimens with a lower fiber volume fraction produced a higher fracture toughness then specimens with higher fiber volume fractions.

**Joining Composite Sandwiches**

Joints often become necessary when assembling several composite sandwich panels. Connections between two structural members represent a zone of potential weakness in the context of composite materials. This is particularly true when the two members are perpendicular to one another. In this case, load is transferred from one member to the other in an out-of-plane mode [6]. In aerospace structures, stiffness and strength to weight ratios, and fatigue and corrosion resistance are extremely important and a lot of research has been done to improve these characteristics. De Jong et al. [7] state that a CFRP plate with a hole will delaminate from the stress concentration if it is overloaded, as opposed to an aluminum plate in which the stress concentration will decrease after an overload due to plasticity. This is one reason fastenerless composite designs are desired. Van Rijn [8] reviews four fastenerless designs for closing a composite wing structure: the Hütter-Hänle method where two L-shaped angles are attached to the sandwich wing skin, and a sandwich web is bonded between the angles; the GROB method where the flanges of a pre-cured I beam are bonded to the wing skins at a location where there is a trough in the skins; the Schleicher method which is similar to the GROB method except for the fact that there is no trough in the wing skins; and the Beechcraft method that uses a 3D braided section bonded to both the skins and the web. Van Rijn [8] considers the latter method a well designed solution capable of taking shear as well as perpendicular loads. Currently, much research is being performed to understand the behavior of three-dimensional braids. Sun and Qiao [9] developed a fiber-inclination model to predict strength based on transverse isotropy of unidirectional lamina and the Tsai-Wu polynomial failure criterion. They concluded that the braider

angle has a significant influence on tensile modulus and strength, and that axial yarns can improve the tensile properties of braided composites. In the second paper of the present Thesis, a 3D braid is manufactured and tested. One of the applications of this braid is to join composite panels.

**References**

[1]. DIAB. ProBalsa Technical Manual, 10.00. DIAB AB, Box 201, S-312 22 Laholm, Sweden (also available at http://www.diabgroup.com).

[2]. DIAB. Divinycell H-Grade Technical Manual, 10.00. DIAB AB, Box 201, S-312 22 Laholm, Sweden (also available at http://www.diabgroup.com).

[3]. Majumdar, P., Srinivasagupta, D., Mahfuz, H., Joseph, B., Thomas, M., Christensen, S., 'Effect of processing conditions and material properties on the debond fracture toughness of foam-core sandwich composites: experimental optimization,' Composites Part A: Applied Science and Manufacturing, Vol. 34, Issue 11, pp. 1097-1104, 2003.

[4]. Chen, H., Bai, R., 'Post buckling behavior of face/core debonded composite sandwich plate considering matrix crack and contact effect,' Composite Structures, Vol. 75, pp. 305-313, 2002.

[5]. Li, X., Carlsson, L., Davies, P., 'Influence of fiber volume fraction on mode III interlaminar fracture toughness of glass/epoxy composites,' Composites Science and Technology, Vol. 64, pp. 1279-1286, 2004.

[6]. Junhou, P., Shenoi, R.,'Examination of key aspects defining the performance characteristics of out-of-plane joints in FRP marine structures, Composites Part A, Vol. 27A, pp. 86-103, 1996.

[7]. de Jong, T., Beukers, A., and Vogelsang, L., Weight reduction as an added benefit. In 'Fatigue of Aircraft Materials,' Proceedings of the specialists conference dedicated to the 65th birthday of Professor J. Schijive, Delft University Press, 1992.

[8]. L. P. V. M. van Rijn, 'Towards the fastenerless composite design,' Composites Part A, Vol. 27A, pp. 915-920, 1996.

[9]. Sun, H., Qiao, X., 'Prediction of the mechanical properties of three-dimensionally braided composites,' Composites Science and Technology, Vol. 57, pp. 623-629, 1997.

# INFLUENCE OF FACE/CORE INTERFACE AND RESIN ON DEBOND TOUGHNESS OF FOAM AND BALSA CORED SANDWICH

A. Truxel[2], F. Avilés[1], J. Grenestedt[2], L.A. Carlsson[1], K. Millay[1]

[1] Department of Mechanical Engineering

Florida Atlantic University

Boca Raton, FL 33431.

[2] Department of Mechanical Engineering

Lehigh University

Bethlehem, PA, 18015

---

## ABSTRACT

Sandwich face/core interfaces were manufactured in five different ways for two different cores. The Tilted Sandwich Debond (TSD) test was used to measure the debond fracture toughness. There was roughly a 60% increase in fracture toughness from the method producing the lowest to the method producing the highest fracture toughness. The foam cored specimens, on average, produced approximately 50% higher fracture toughness than the balsa cored specimens. Regardless of core, using continuous filament mat between the core and fibers produced the highest fracture toughness.

---

## Introduction

Presently there is a trend towards making stronger, more lightweight and more cost effective structures. These structures can be found in aerospace, navel, automotive and public transportation vehicles, bridges and other civil infrastructure, and sporting equipment. Composite sandwich structures are particularly well suited for aerospace and marine vehicles because of high strength and stiffness to weight ratios, high corrosion and fatigue resistances, and the ability to be manufactured into complex shapes.

Composite sandwich structures generally consist of a low density core between two high strength and stiffness face sheets. The thicker the core, the further the skins are from the neutral axis, making the sandwich stronger and stiffer in bending. The skins take the majority of the in-plane and bending loads, while the core takes shearing loads and prevents sandwich panels with thin skins from wrinkling. The strength of the sandwich is greatly dependent upon the face/core interface and how it was manufactured. If there is a poor bond between the core and the face sheets, then the strength of the sandwich is reduced and the face sheets could debond. If a chain is only as strong as its weakest link, then a composite sandwich panel may be only as strong as its weakest face/core interface.

The face/core interface of a composite sandwich panel is a very important part of the panel's integrity. The manner in which the interface was manufactured is also very important. The Diab Divinycell H-Grade and ProBalsa Technical Manuals [1, 2] advise vacuum cleaning and priming the cores prior to vacuum infusion. Using a vacuum

cleaner instead of, for example, compressed air to reduce the risk of oil from the air line to contaminate the interface, would affect the adhesion. Priming the core with, for example, a coating of quick curing resin may reduce the risk that the core drains excessive amounts of resin from the skins and thus creates a resin starved interface. The author could not find a comparison of how different methods of resin infusion affect the face/core interface. However, there has been a lot of research done on modeling and testing the interface. Various methods to test the interface have been proposed. Grenestedt introduced the Tilted Sandwich Debond (TSD) method, which was later studied in detail by Li et al. [5]. Majumdar et. al. [3] studied the effects of temperature processing, suction, and foam density on the debond fracture toughness using the TSD test method. Li et al., [5] concluded that specimens with a lower fiber volume fraction produced a higher fracture toughness then specimens with higher fiber volume fractions. This has some relation to results of the present study.

## Materials

Two different core materials were used for the study, H200 Divinycell semi-rigid PVC foam and ProBalsa Standard (155 kg/m$^3$) density kiln-dried end-grain balsa wood, each measuring 25.4 mm thick. The core material properties are listed in Table 1 [1, 2]. The reinforcement used was Owens Corning Knytex WR24-5x4 bi-directional (0°/90°) glass fiber weave. The fabric weight was 815 g/m$^2$, with 440 g/m$^2$ in the 0° direction and 375 g/m$^2$ in the 90° direction. The material properties are shown in Table 2 [6]. The matrix was Dow Derakane 8084 vinyl ester epoxy resin, mixed with Cobalt Naphthenate-6%

(CoNap), Dimethylaniline (DMA), Methylethylketone peroxide (MEKP), and 2, 4-Pentanedione (2, 4-P). The CoNap and DMA were used to promote the reaction, MEKP is the hardener, and 2, 4-P is an inhibitor used to increase the gel-time. The weight percentages added of each chemical recommended by the manufacturer for 80 °F are as follows: 1.5% MEKP, 0.025% DMA, and 0.15% CoNap [7]. With 2, 4-P, more CoNap is recommended and 0.2% CoNap was used. The amount of 2, 4-P added varied depending on the desired gel time. The panels processing is briefly discussed in the next Section, after which the particulars of the interface are discussed.

**Interface Preparation and Panel Processing**

The goal of the experimental study was to investigate face/core bond strength between two different core materials (foam and balsa), each using five different interface preparations. The interface preparations had to do with the manner in which resin was infused into the fibers. The different ways resin was infused are as follows: two different patterns of grooves in the core, a layer of Resin Distribution Medium (RDM) on top of a peel ply over the fibers, a layer of Continuous Filament Mat (CFM) between the fibers and the core, and nothing to speed up the resin flow but an inhibitor (2, 4-P) added to the resin to delay the gel-time. The five configurations were:

1. Grooves in the core, 2 mm wide and 4 mm deep in a 40x40 mm grid,
2. Grooves in the core, 2 mm wide and 2 mm deep in a 20x20 mm grid,
3. Resin Distribution Medium and peel ply on top of the fibers,
4. Continuous filament mat between the core and the fibers,

5. Resin Inhibitor (2, 4-P).

The first two configurations, with grooves in the cores, had the same volume of resin grooves per unit area of foam core. The mass added due to resin in the grooves would thus be the same for these two. Channels connecting the grooves to a resin runner were cut on the sides of the cores. The resin was introduced in this runner during the vacuum infusion. Vacuum was drawn from the opposite side of the panel. The resin thus flowed from the resin runner to the grooves in the top of the core, wicking up through the fibers, and continuing towards the vacuum port. Since the resin flowed through grooves at the core/fiber interface *first*, gas bubbles tended to flow away from the fiber/core interface. However, the resin fills the grooves surrounding all 20x20 mm or 40x40 mm squares before the fabric over that square has been completely saturated. This leads to a non-saturated area within each square. The bonding between the core and skin is expected to be reduced due to this. On the other hand, the resin cures in the grooves and this is expected to increase the interfacial bond strength. Diagrams of configurations 1 and 2 are shown in Figures 1a and 1b.

The third configuration used a resin distribution medium, which is commonly used to reduce infusion time. Peel ply was laid between the fibers and the distribution medium so the latter could be removed after the resin cured. This method is lighter then grooves (Configurations 1 and 2) and continuous filament mat (Configuration 4) since the resin distribution medium is removed after the part has cured. The resin distribution medium, peel ply, and additional resin wicked up by the distribution medium, add cost to the part.

The resin distribution medium was connected to the resin runner at the side of the core. The resin flowed quickly through the distribution medium and then slowly through the thickness of the fibers toward the core. Consequently, gas bubbles and other contaminations at the flow front tend to accumulate at the core/fiber interface. On the other hand, the non-saturated areas as found in Configurations 1 and 2 were not seen. A diagram of configuration 3 is shown in Figure 1c.

The fourth configuration had a layer of Owens Corning M-8610 (450 $g/m^2$) continuous filament mat between the core and fibers. This mat has high permeability and resin thus flows quickly through it. The mat was connected to the resin runner on the side of the core. The mat allows the resin to flow quickly and evenly wet-out the core/fiber interface. This method lends itself to a good core/fiber interface since there is less of a chance for dry spots compared to grooves. The resin rich mat is expected to have better through-the-thickness strength than obtained with woven fabrics. Further, the continuous filament mat may act as at stiffness gradient between the soft core and the stiff skin. However, the mat adds thickness to the skins and considerable weight to the panel. A diagram of configuration 4 is shown in Figure 1d.

The fifth configuration did not have any grooves or other form of resin distribution medium*. The infusion time was thus considerably longer than for the other configurations. To ensure that the resin did not gel before fully infusing the panel, enough of the inhibitor 2, 4-P was added to the resin to delay the gel time to 4-5 hours. This method does not have the added weight of grooves, distribution medium or continuous

filament mat and there were minimal dry spots and air bubbles since the resin slowly and uniformly moves through all the fibers with any bubbles moving towards the flow front. A diagram of configuration 5 is shown in Figure 1e.

*A small amount of distribution medium was used on the side of the core to help the resin flow from the resin runner to the fibers.

In an effort to minimize variability, each core was cut from one sheet of material. Each 610 x 1220 mm sheet was cut into two pieces, one smaller piece for specimens with the fifth configuration containing only 2, 4 –P and one larger piece for specimens with the remaining four configurations. A CNC router was used to cut the two pieces and machine the grooves. The cores were not primed or treated but compressed air was used to clean off any dirt or dust and the grooves were cleared of any obstructions. The foam core is shown in Figure 2 after the interface was prepared but before the fibers were placed.

The skins of all panels consisted of eight layers of the glass fiber fabric. The fabrics were all oriented such that the 0° direction was parallel to the longer side of the core. After all materials were laid up on the core, a vacuum bag was placed on top and sealed to a release agent coated steel plate under the assembly. Air was evacuated and the vinyl ester was infused. All configurations, except the fifth one containing only 2, 4-P, were done with one infusion for each core. This means, that four of the five configurations used the same exact vacuum bag, pressure, resin, processing conditions, etc. There were four total infusions, one for the 2, 4 – P configuration and one for the remaining four configurations

for the balsa core and the foam core. For each infusion, the resin was mixed for 5 minutes, degassed for 10 minutes, and then infused at a total pressure of 35 kPa (65% vacuum). One of the infusions is shown in Figure 3. After the panels were fully infused the resin inlet was closed and the vacuum remained on.

The only differences between the four infusions are as follows, the fifth (2, 4-P) configuration for foam used 0.35% 2, 4-P to delay the gel time. This produced too long of a gel time so 0.25% 2, 4 – P was used for the balsa cored 2, 4 – P configuration. The balsa panel was left under vacuum for at least 14 hours before it was infused to allow trapped air in the porous balsa to escape.

All panels were left under vacuum for 24 hours after they were infused. The panels were then de-molded and cut using an abrasive water jet cutter, Fig. 4. There were ten specimens tested from each of the five configurations for the two different cores making a total of 100 specimens. Each specimen was 40 mm wide by 130 mm long. For the grooved configurations the specimens were cut out so the grooves were aligned down the center. A specimen side view of each configuration is shown in Figure 5.

**Determination of Debond Fracture Toughness**

The tilted sandwich debond (TSD) specimen, introduced by Grenestedt and later analyzed in detail by Li and Carlsson [1999], was used for debond fracture characterization. The TSD specimen has an initial crack at the interface between the top

face and the core. A vertical pulling load, P, is applied at the (debonded) top face to promote crack growth, Fig. 6.

The magnitude of the applied load, P, is increased until face/core debonding occurs. It has been recently demonstrated that the firm attachment of the lower part of the specimen to the base favors interfacial crack growth [Carlsson et al., 2005]. Figure 7 shows a schematic of the actual TSD test rig utilized, with a sandwich specimen mounted on the vice. The use of a tiltable vice allows for loading of the TSD specimen at different tilt angles. Previous studies, however, have shown that the tilt angle has minor influence on the mode mixity and crack propagation path [Li and Carlsson, 2001; Viana and Carlsson, 2003]. In this study, the vice was fixed at a zero degree angle.

A hinge tab bonded to the top face of the TSD specimen at the end of the precracked portion allows for moment-free vertical load application, see Fig. 7. The test fixture was placed in a Tinus-Olsen DS-50 displacement controlled test frame, with a 1.3 kN load cell. Load was applied to the sandwich specimen by displacing the cross-head until the crack propagated (stable or unstable) and stopped at a new crack length. A crosshead displacement velocity of 1.2 mm/min was used thorough the test. The displacement was measured using a calibrated linear variable differential transducer (LVDT), located at the cross-head. A load-displacement (P-$\delta$) curve was recorded using the load signal from the test machine and the displacement from the LVDT. Once the initial crack propagated and stopped, the new crack length was marked on the specimen edge for posterior measurement and the specimen was unloaded completely. This process was repeated for

each new crack length until the top face of the sandwich specimen became totally separated from the core. Three to seven crack lengths were required to cause total face/core separation.

**Data Reduction for TSD Fracture Test**

The experimental compliance calibration method was used to obtain the debond fracture toughness, $G_C$, from the TSD test data. In this method, the compliance ($C = \delta/P$) of the TSD specimen is evaluated from the initial slope of the load-displacement (P-δ) record at each crack increment ($da$). Thus, a set of compliance data for various crack lengths is obtained. This compliance data is curve-fitted versus the crack length with an $n$-th order polynomial,

$$C = \sum_{i=0}^{n} \beta_i a^i = \beta_0 + \beta_1 a + \beta_2 a^2 + .... + \beta_{n-1} a^{n-1} + \beta_n a^n \qquad (1)$$

Once a calibrated compliance curve is established, $G_C$ can be calculated (for each crack length) from the change of compliance with crack length, the specimen width ($b$) and the critical load at crack propagation ($P_C$), as

$$G_C = \frac{P_C^2}{2b}\frac{dC}{da} = \frac{P_C^2}{2b}\sum_{i=1}^{n} i\beta_i a^{i-1} = \frac{P_C^2}{2b}\left(\beta_1 + 2\beta_2 a. + .... + n\beta_{n-1} a^{n-1}\right) \qquad (2)$$

In such a way, a fracture toughness value, $G_C$, is obtained at each crack length for the same specimen. It is important to point out that the value of $G_C$ at the initial crack length depends very much on the way in which the initial crack was produced. Therefore, the

initial value may be rather different from the average and is frequently disregarded. Also, as observed by Shivakumar et al. [Shivakumar et al., 2005], end effects are likely to disrupt the compliance fitting for very large cracks.

**Specimen Preparation**

Large sandwich panels (with a single face sheet) were manufactured as explained before and cut into TSD specimens. The final dimensions of the TSD specimens were 40 mm wide and 130 mm long, with a thickness of approximately 30 mm (25.4 mm for the core and approximately 5 mm for the face sheet). Since the bottom face sheet was not required for TSD testing, the exposed (bottom) surface of the core was adhesively bonded to a steel (base) plate using an epoxy adhesive (3M Scotch-Weld, 1751 A/B), as is shown in Fig. 8. This base plate was bolted to the vice of the test fixture, see Fig 8. Prior to bonding, the bonding surface of the base plate was sanded and cleaned with acetone, promoting good adhesion. A 25 mm wide piano hinge was bonded to the face sheet using the same roughening/cleaning procedure and same epoxy resin as for the base plate. The hinge was bonded with its edge flush with the specimen end, placing the hinge rotation axis (load application point) 38 mm from the specimen edge, see Fig. 8.

The specimens were precracked using a two-step procedure. First, a table saw with a 0.8 mm thick saw blade was used to cut the initial crack. The crack tip was then sharpened and extended with a thin (0.3 mm) cutter blade. The nominal length of the initial crack, measured from the load application point, $a_0$ in Fig. 8, was nominally 35 mm with ±1 mm of deviation. It is important to point out that, given the tough nature of the foam (H200)

and balsa cores, the amount of sharpening in the pre-crack was limited. Although the pre-crack was aimed to be at the actual face/core interface, the crack tip (after sharpening) was commonly located in the core, slightly underneath the interface. Measurements of the crack length were done with a digital Mitutoyo caliper of 0.01 mm resolution, and the crack length was averaged from readings on both sides of the TSD specimen. The specimens were labeled according to the manufacturing configuration used for the face/core interface, see Table 3. Three replicates for each configuration (grooves 2x4-40, grooves 2x2-20, RDM, CFM, 2-4P) and each core were tested, making a total of 30 TSD specimens (15 for balsa and 15 for H200).

## Results and Discussion

### *Crack Growth Path*

The characteristics of the crack propagation path were visually monitored. The overall tendency of the crack was to propagate at or near the face/core interface in a stick-slip (unstable) manner. However, differences were observed depending on the core type and specimen configuration.

Regarding the balsa core specimens, the crack paths of the two configurations with grooves (2x4(40) and 2x2(20) in Table 4) were very similar. For these specimens, the crack meandered around the interface, propagating at or very near the face/core interface in regions where the bond between the face and core was relatively weak, but kinked into the core and propagated slightly underneath the face/core interface in regions where the

resin was able to penetrate the core and form a strong bond, see Fig. 9a. These local regions of strong face/core bonding were particularly obvious at the grooves located transversely to the crack growth (along the specimen width). It was observed that the crack was temporarily arrested when it encountered a groove across its path. After crack arrest, the crack either veered around the groove or broke across it, see schematic in Fig. 10. When the crack circumvented the groove by veering around it, propagating down into the core and underneath the groove, and then back to the interface once the crack had passed the groove, see schematic in Fig. 10a. In some instances, however, the crack broke across the groove, Fig. 10b, which required equal or larger amount of energy (applied load) than its preceding crack, as will be shown later. For the rest of the configurations with balsa core (RDM, CFM, and 2,4-P) the crack propagated at or near the face/core interface with a minimum tendency of kinking into the core. In particular, the balsa cored configuration using resin distribution medium (RDM) showed increased tendency for interfacial crack growth, see Fig. 9b.

The H200 foam cored specimens with grooves (2x4(40) and 2x2(20) in Table 5) presented crack propagation paths at or near the face/core interface for the major part of the specimen, Fig. 11a. Both grooved configurations presented very similar crack propagation behavior. After crack arrest by a transverse groove, the crack mostly broke across the groove, assumed to be due to the higher toughness of the H200 core, Fig. 10a. In a few cases, however, slight crack kinking into the core was seen, Fig. 10b, but the crack kinked back towards the interface immediately after the groove. Near the end of the specimens, the crack tended to kink into the core (at an angle of approximately $15^0$).

The H200 foam cored specimens with RDM, CFM, and additional inhibitor (2,4-P), presented similar crack growth. For such specimens, the crack propagated as a sub-interface crack 0.5-2 mm below the face/core interface, until the end of the specimen was approached, Fig. 11b. Near the end of the specimen, the crack kinked into the core and the face debonded completely from the core.

After testing, the crack surfaces of the separated face sheets were examined, Fig. 12a. The balsa cored specimens with grooves (2x4 and 2x2 mm) showed local adherence of balsa core near the grooved regions. The post-mortem examination showed that such grooves were filled with resin (and some air bubbles), forming a local strong bond between the face and core. Occasional long, isolated, peaks of balsa were pulled out from the core. The separated faces of the RDM, CFM and 2,4-P specimens show only few traces of balsa, Fig. 12a. The RDM showed a neat face/core interface without balsa core traces. The continuous fibers were clearly visible on the faces of the balsa specimen with CFM, and the weave pattern of the glass fibers were observed on the faces of the 2,4-P specimen, highlighting the interfacial behavior of the crack path on those specimens.

For the specimens with H200 foam core, Fig. 12b, the post-mortem examination of the grooved specimens showed only limited amount of core traces for the first part of the face sheet (a = 0 to 45 mm). The amount of foam on the face sheet was seen to increase as the specimen approached to its end (lower end in Fig. 12). As mentioned above, near the end of the specimen the crack tended to kink into the core, leaving a tapered core

layer on the face sheet. The specimens with RDM, CFM and additional inhibitor (2,4-P) showed a 0.5-2 mm layer of foam core on the surface of the debonded face, corroborating sub-interfacial crack growth.

*Load-Displacement Response*

Figures 13 and 14 show load-displacement curves for each crack length of representative TSD specimens with balsa core, Fig. 13, and foam core, Fig. 14. The curves are fairly linear prior to crack growth, when the load drops sharply at a critical load $P_C$, corresponding to the onset of crack propagation. Overall, the critical load was observed to decrease with increased crack length, as expected, but some peculiarities were observed for the different configurations. For the balsa cored specimen with 2x4 mm grooves in a 40x40 mm pattern, Fig. 13a, the critical load was observed to decrease with increased crack length for the first five crack lengths, as expected. For this specimen, the fifth crack propagated at a critical load of about 250 N and was arrested by a transverse groove. Thus, the sixth curve corresponds to a crack with its flank in front of one of the grooves, and the load required to propagate that crack across the groove was similar to that of the preceding crack (near 250 N). A similar behavior was observed between the third and fourth cracks of the balsa specimen with 2x2 mm grooves, Fig. 13b. For this specimen, the third crack was arrested by a groove and the load required to propagate such an arrested crack further ($P_C$ in fourth curve) was similar to the critical load of the previous (third) crack. When the crack overcame the groove by kinking below it, the critical load did not show an increase, as may be expected since the propagation was in

the core. The specimens that were manufactured only with resin distribution medium (RDM) showed more conventional P-δ curves, Fig. 13c, but with larger (unstable) crack jumps. This was expected since the cracks were allowed to propagate freely, without grooves or any other crack arresting mechanism. The balsa specimens with continuous fiber mat (CFM) at the face/core interface, Fig. 13d, and additional inhibitor (2,4-P), Fig. 13e, showed higher values of $P_C$ than the grooved and RDM ones, indicating a strong face/core interface. However, the CFM specimens were thicker and stiffer, so comparing forces is not a true indication of interface toughness.

The behavior of the specimens with H200 foam core was qualitatively similar to that for their corresponding configurations with balsa wood core: the grooved specimens, Fig. 14a and b, showed increased $P_C$ when the crack passed across a groove; the RDM specimens showed typical crack growth (with cracks propagating longer); and the CFM and 2,4-P specimens showed a higher critical load compared to corresponding balsa cored configurations with the same crack lengths. The critical loads to propagate the cracks for the H200 cored specimens, however, were substantially higher than those for the balsa cored specimens.

*Compliance, Resistance Curves and Debond Toughness*

In order to implement the experimental compliance calibration method for determination of fracture toughness, the compliance ($C = \delta/P$) was calculated at each crack length for each of the specimens examined. A polynomial was curve fit using Eq. (1) for each

specimen. The polynomials were curve fit using the least squares method. A third order polynomial provided good fitting. Figure 15 shows a typical compliance vs. crack length (*C-a*) curve for a balsa cored CFM specimen.

The debond fracture toughness, $G_C$, was calculated for each crack length using the compliance curves and Eq. (2). Figure 16 shows $G_C$ vs. crack length (R-curves) for representative TSD specimens with balsa (Fig. 16a) and H200 (Fig. 16b) cores.

The grooved configurations (2x4 and 2x2) showed quite a large scatter of the debond fracture toughness data within the same specimen (for different crack lengths). As explained before, the transverse grooves arrested the crack growth causing relative large variations in the fracture toughness for the same specimen. Regardless of the core type, the RDM, CFM, and 2,4-P configurations showed $G_C$ values that tended to fluctuate around an average, within the same specimen, without as much scatter as the grooved specimens. The first value of $G_C$ normally scatters as a result of variability in the precracking procedure and sharpness of the artificial tip. Further, the last crack tended to kink into the core, which appeared to reduce the value of Gc for such a crack length. Thus, the initial and last values of Gc were disregarded when calculating the average fracture toughness. The average debond fracture toughness and standard deviation were calculated from the values of $G_C$ for each crack length and all replicates. Table 4 presents the average debond fracture toughness and standard deviation for the TSD specimens with balsa wood core. Table 5 presents the corresponding values for specimens with H200 PVC foam core.

The fracture toughness of the configurations with H200 core was higher than the corresponding values for balsa wood core, showing a core influence in the fracture toughness. It is important to remind, however, that crack propagation in the balsa cored specimens was at or near the face/core interface, while the H200 specimens showed mostly sub-interfacial crack growth. The same qualitative trends were observed for both cores. For a given core material, the grooved configurations showed similar values of $G_C$. In spite of the local peaks of $G_C$ for the grooved specimens, their average value was similar to that for the RDM configuration (around 0.85 $J/m^2$ for balsa and 1.4 $J/m^2$ for H200 foam). The configuration containing a continuous fiber mat (CFM) at the face/core interface showed the highest $G_C$, followed by the configuration that used additional inhibitor (2,4-P) to increase the resin gel time. The fiber mat in the CFM configuration lead to increased toughness, but at the expense of increased weight. Increased gel time (2,4-P), however, was observed to produce high toughness without any weight penalty.

It is important to point out that the relative large standard deviation of the grooved specimens observed in Table 5 comes mostly from scattered data within the same specimen, see R-curves in Fig. 16. The majority of the standard deviation of the RDM, CFM, and 2,4-P configurations, on the other hand, arises from scattered average between replicates, since the scattering within the same replicate was not too large, see R-curves in see Fig. 16.

## Discussions and Conclusions

Sandwich face/core interfaces were manufactured in five different ways for two different core materials. The Tilted Sandwich Debond (TSD) test was used to measure the debond fracture toughness. On average, the debond fracture toughness of the foam cored panels was roughly 60% higher than the balsa cored. The configuration producing the highest fracture toughness was roughly 50% higher than the configuration producing the lowest fracture toughness, regardless of core material. This suggests that the type of core used and the method of interface manufacture has a substantial effect on the debond fracture toughness. The configurations with continuous filament mat and 2, 4-P had the highest and second highest debond fracture toughnesses for each core. A few conjectures why continuous filament mat produce specimens with higher debond fracture toughness are: the continuous filament mat produces a resin rich interface and the resin has a higher transverse tensile strength than the woven composite (as previously mentioned, specimens with a higher resin content produce higher fracture toughness compared to specimens with lower resin content, Li et al., [5]); since continuous filament mat has a high resin content, there is less risk that the interface becomes resin starved if the core drains excessive amounts of resin from the skins; and impurities and air bubbles that are often found at the resin flow front tend to flow through the mat towards the vacuum port and thus not end up in the interface.

The grooved specimens had a sharp increase in Gc and the crack kinked into the core where the transverse grooves were located. The balsa cored grooved specimens had

isolated peaks of balsa pulled out of the core. The foam cored grooved specimens had cracks that mostly penetrated across the grooves. In the other configurations (without grooves), the cracks propagated at or near the face/core interface.

**References**

[1]. DIAB. ProBalsa Technical Manual, 10.00. DIAB AB, Box 201, S-312 22 Laholm, Sweden (also available at http://www.diabgroup.com).

[2]. DIAB. Divinycell H-Grade Technical Manual, 10.00. DIAB AB, Box 201, S-312 22 Laholm, Sweden (also available at http://www.diabgroup.com).

[3]. Majumdar, P., Srinivasagupta, D., Mahfuz, H., Joseph, B., Thomas, M., Christensen, S., 'Effect of processing conditions and material properties on the debond fracture toughness of foam-core sandwich composites: experimental optimization,' Composites Part A: Applied Science and Manufacturing, Vol. 34, Issue 11, pp. 1097-1104, 2003.

[4]. Chen, H., Bai, R., 'Post buckling behavior of face/core debonded composite sandwich plate considering matrix crack and contact effect,' Composite Structures, Vol. 75, pp. 305-313, 2002.

[5]. Li, X., Carlsson, L., Davies, P., 'Influence of fiber volume fraction on mode III interlaminar fracture toughness of glass/epoxy composites,' Composites Science and Technology, Vol. 64, pp. 1279-1286, 2004.

[6]. Owens Corning. Kyntex Woven Rovings Technical Data Sheet. ONE OWENS CORNING PARKWAY TOLEDO, OHIO 43659 (also available at http://secure.owenscorning.net).

[7]. Dow Derakane. Technical Data Sheet for Derakane 8084 Resin. PO Box 2219 Columbus, OH 43216, USA (also available at http://www.derakane.com).

**Tables**

Table 1 Core Material Properties [1, 2]

| Material Properties | | | |
|---|---|---|---|
| **Quality** (ASTM Test Procedure) | | **ProBalsa** | **H200** |
| **Density** (PB:C 271 H200:D 1622) | $kg/m^3$ | 155 | 200 |
| **Compressive Strength** (PB:C 365 H200:D 1621) | MPa | 12.7 | 4.4 |
| **Compressive Modulus** (PB:C 365 H200:D 1621-B) | MPa | 4100 | 310 |
| **Tensile Strength** (PB:C 297 H200:D 1623) | MPa | 13.5 | 6.4 |
| **Tensile Modulus** (PB: N/A H200:D 1623) | MPa | * | 230 |
| **Shear Strength** (PB:C 273 H200:C 273) | MPa | 3 | 3.3 |
| **Shear Modulus** (PB:C 273 H200:C 273) | MPa | 166 | 85 |
| **Shear Strain** | % | * | 33 |

*Data not available

Table 2 WR24-5x4 Knytex glass fiber typical material properties [3]

| Material Properties of Laminate based on 50% glass content by weight | | |
|---|---|---|
| Tensile Strength | MPa | 289 |
| Tensile Modulus | GPa | 14.3 |
| Compression Strength | MPa | 230 |
| Compression Modulus | GPa | 15.7 |
| Flexural Strength | MPa | 385 |
| Flexural Modulus | GPa | 15.2 |

Table 3 Specimen numbering

| Config. # | Description | Specimen # | |
|---|---|---|---|
| | | Foam | Balsa |
| 1 | Grooves 2x4mm with 40mm spacing | 1-10 | 51-60 |
| 2 | Grooves 2x2mm with 20mm spacing | 11-20 | 61-70 |
| 3 | Resin Distribution Medium | 21-30 | 71-80 |
| 4 | Continuous filament mat between the core and fibers | 31-40 | 81-90 |
| 5 | Resin Inhibitor (2, 4 P) | 41-50 | 91-100 |

Table 4 Debond fracture toughness for specimens with Balsa core.

| Specimen | $G_C$ (kJ/m$^2$) | |
|---|---|---|
| | Average | St. Dev. |
| Grooves 2x4-40 | 0.85 | 0.13 |
| Grooves 2x2-20 | 0.81 | 0.16 |
| RDM | 0.93 | 0.25 |
| CFM | 1.31 | 0.30 |
| 2,4P | 1.27 | 0.28 |

Table 5 Debond fracture toughness for specimens with H200 foam core.

| Specimen | $G_C$ (kJ/m$^2$) | |
|---|---|---|
| | Average | St. Dev. |
| Grooves 2x4-40 | 1.36 | 0.30 |
| Grooves 2x2-20 | 1.48 | 0.18 |
| RDM | 1.45 | 0.47 |
| CFM | 2.05 | 0.32 |
| 2,4P | 1.89 | 0.14 |

**Figure Captions**

Fig. 1a. Diagram of configuration 1 (2 x 4mm grooves with 40 mm spacing).

Fig. 1b. Diagram of configuration 2 (2 x 2mm grooves with 20 mm spacing).

Fig. 1c. Diagram of configuration 3 (Resin distribution medium).

Fig. 1d. Diagram of configuration 4 (Continuous filament mat).

Fig. 1e. Diagram of configuration 5 (No method used to quickly introduce resin, just inhibitor (2, 4-P used to prevent the resin from gelling).

Fig. 2. Foam with continuous filament mat and grooves.

Fig. 3 Panel being infused.

Fig. 4. Cutting the specimens to size using an abrasive water jet cutter.

Fig. 5 Side view of each specimen configuration before testing.

Fig. 6 Principle of the TSD specimen.

Fig. 7 TSD test rig.

Fig. 8 Sketch of a TSD specimen.

Fig. 9 Crack propagation in selected balsa cored specimens during actual testing.

a) 2x2 (20) grooved b) resin distribution medium.

Fig. 10 Schematic of crack path in front of a groove.

a) Around the groove, b) across the groove.

Fig. 11 Crack propagation in selected H200 foam cored specimens during actual testing.

a) 2x4 (40) grooved b) resin distribution medium.

Fig. 12 Photos of fracture surfaces (face side) of TSD specimens.

a) Balsa cored, b) H200 foam cored.

Fig. 13 Load-displacement curves for TSD specimens with balsa core.

a) 2x4(40) grooves, b) 2x2(20) grooves, c)RDM, d)CFM, e)2 -P.

Fig. 14 Load-displacement curves for TSD specimens with balsa core.

a) 2x4(40) grooves, b) 2x2(20) grooves, c)RDM, d)CFM, e)2,4-P.

Fig. 15 Compliance curve for a representative specimen (CFM with balsa core).

Fig. 16 R-curves for representative TSD specimens.

a) Balsa cored, b) H200 foam cored.

## Figures

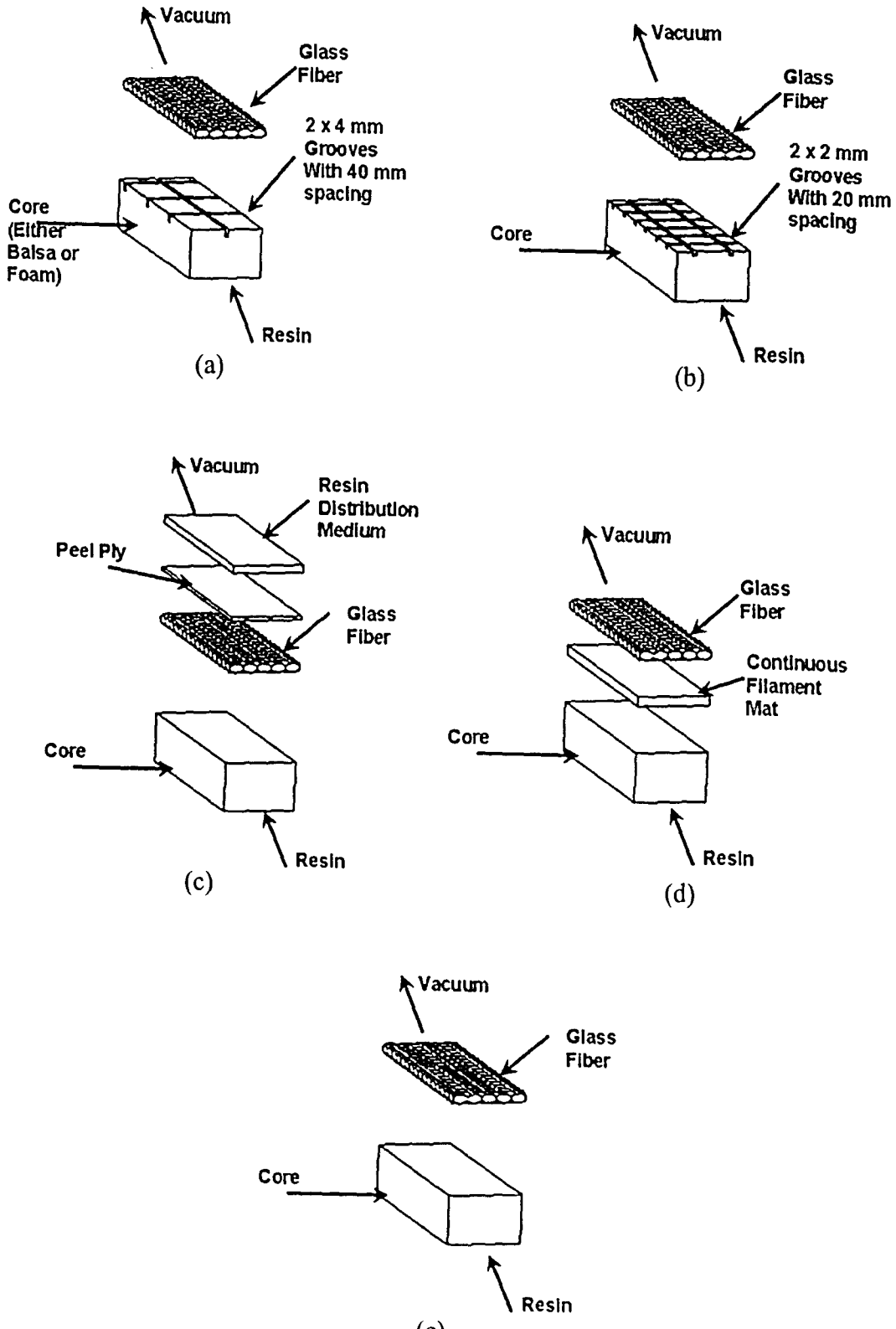


Fig. 1

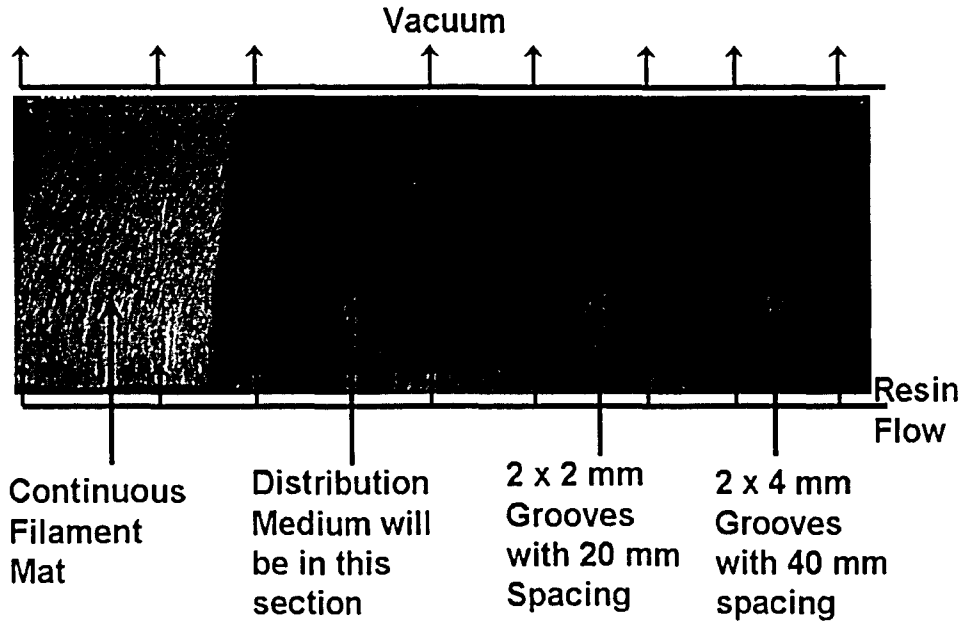
Vacuum
Resin Flow
Continuous Filament Mat
Distribution Medium will be in this section
2 x 2 mm Grooves with 20 mm Spacing
2 x 4 mm Grooves with 40 mm spacing

Fig. 2

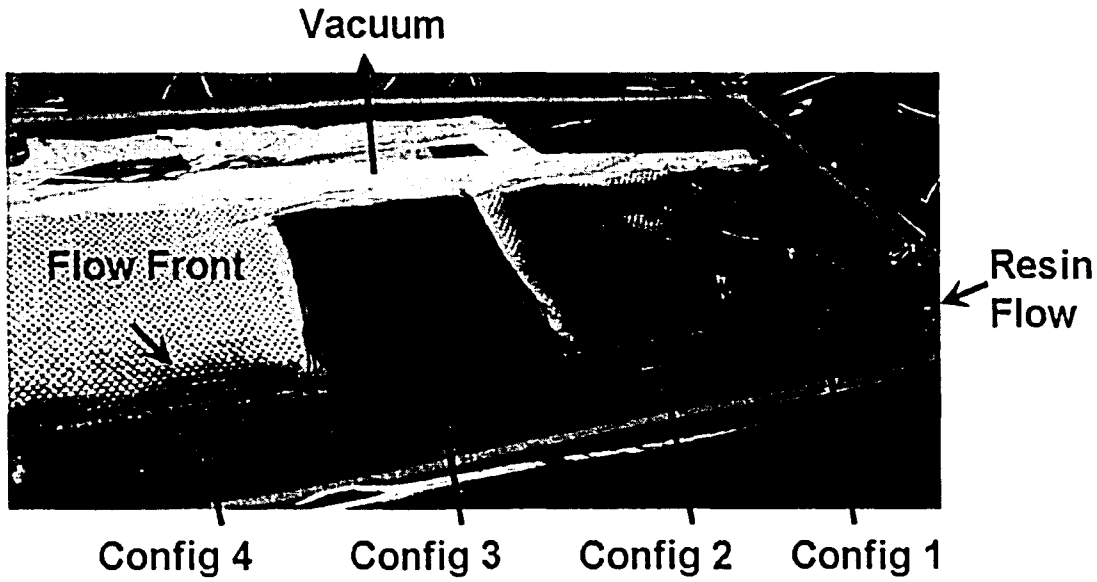
Vacuum
Flow Front
Resin Flow
Config 4
Config 3
Config 2
Config 1

Fig. 3

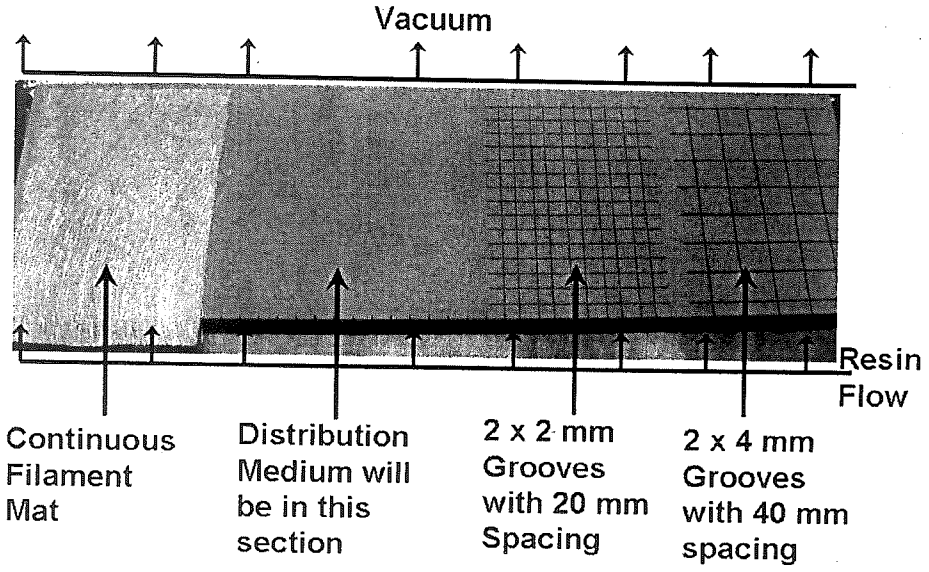
Vacuum
Resin Flow
Continuous Filament Mat
Distribution Medium will be in this section
2 x 2 mm Grooves with 20 mm Spacing
2 x 4 mm Grooves with 40 mm spacing

Fig. 2

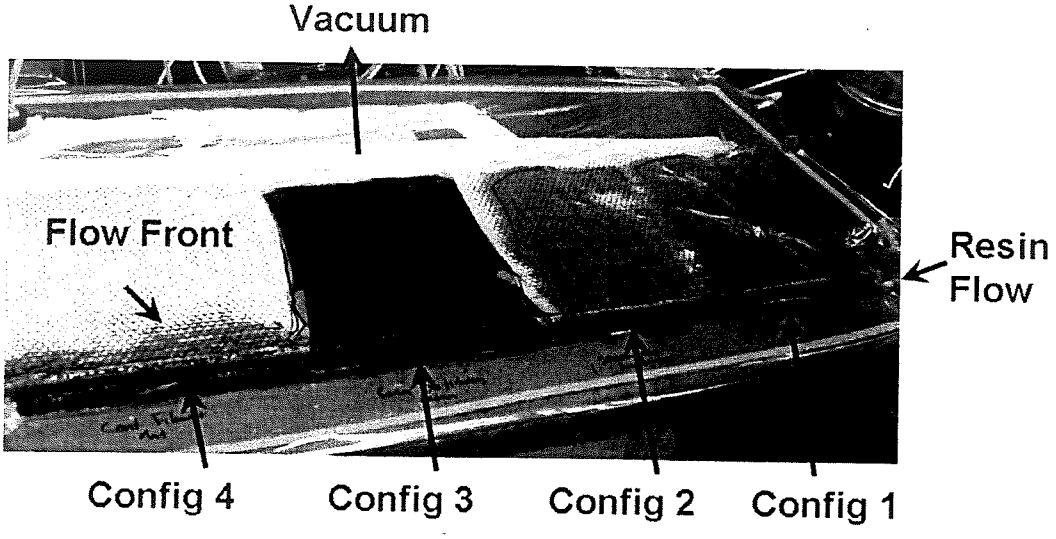
Vacuum
Flow Front
Resin Flow
Config 4
Config 3
Config 2
Config 1

Fig. 3

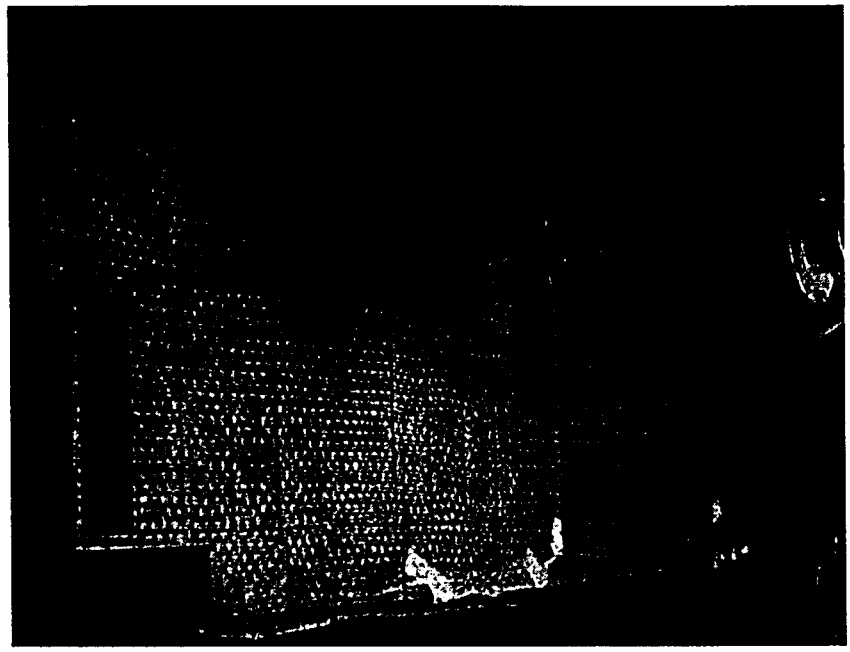

Fig. 4

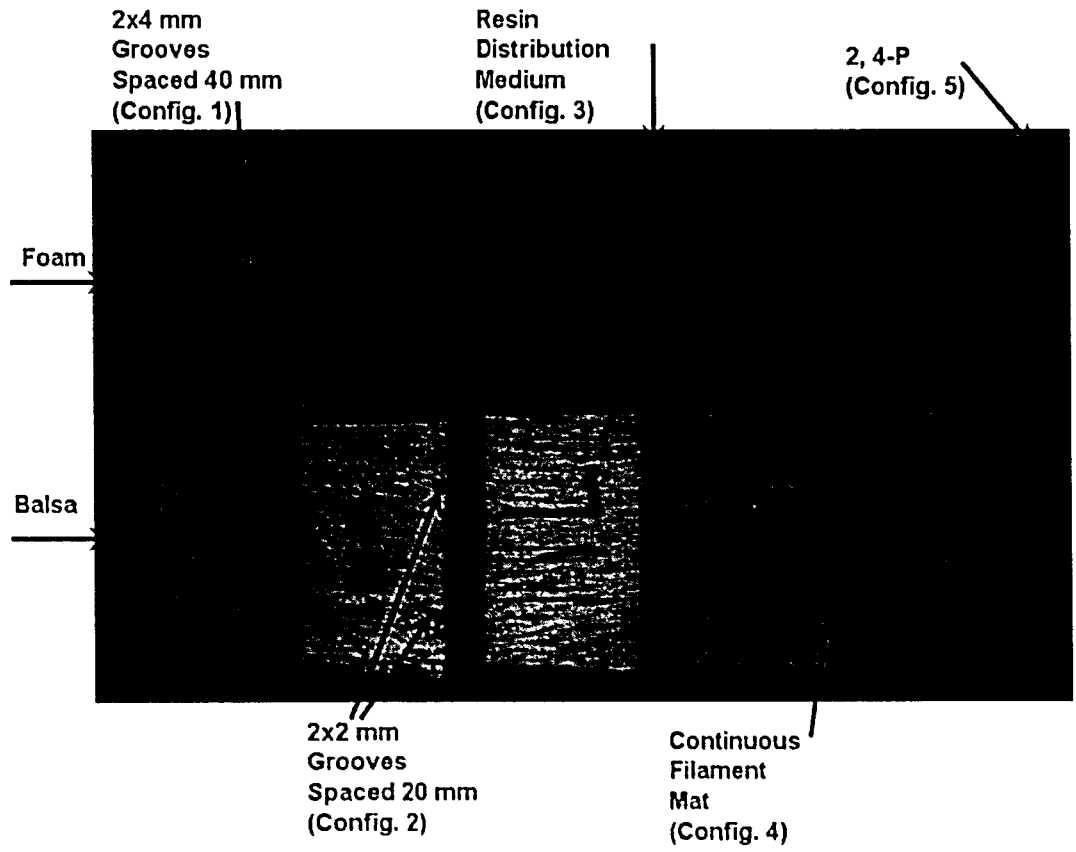
2x4 mm
Grooves
Spaced 40 mm
(Config. 1)
Resin
Distribution
Medium
(Config. 3)
2, 4-P
(Config. 5)
Foam
Balsa
2x2 mm
Grooves
Spaced 20 mm
(Config. 2)
Continuous
Filament
Mat
(Config. 4)

Fig. 5

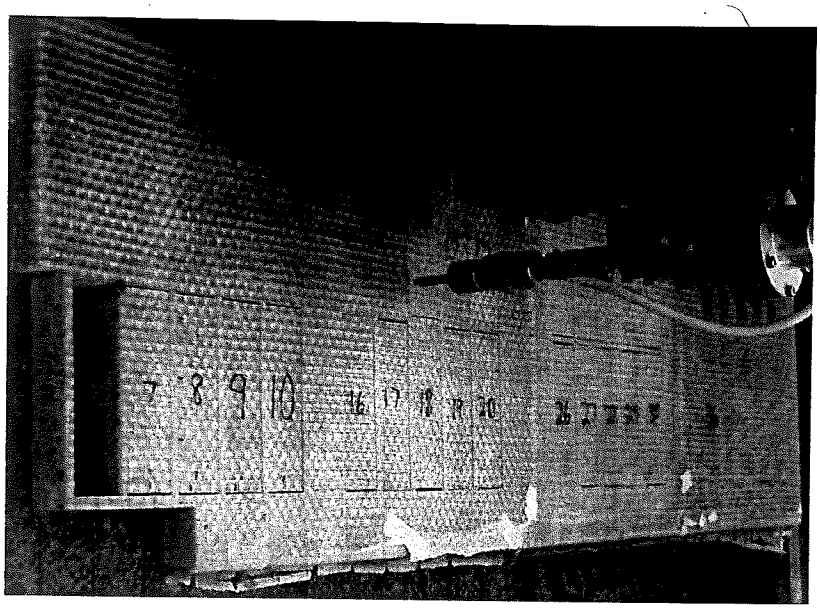

Fig. 4

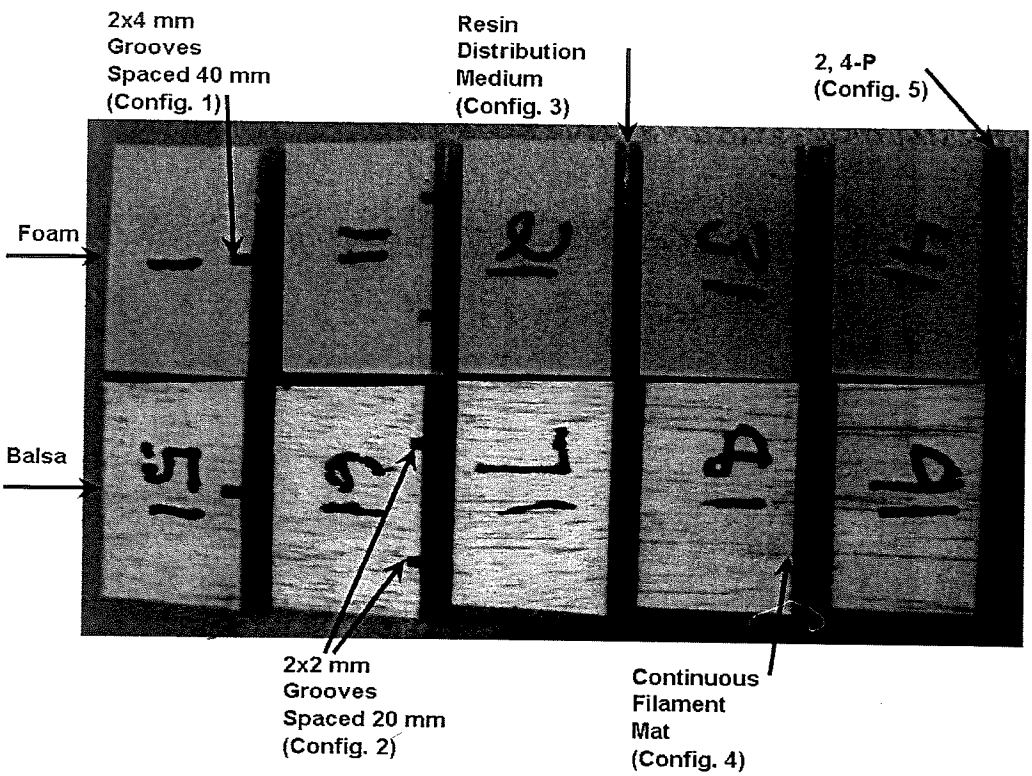


Fig. 5

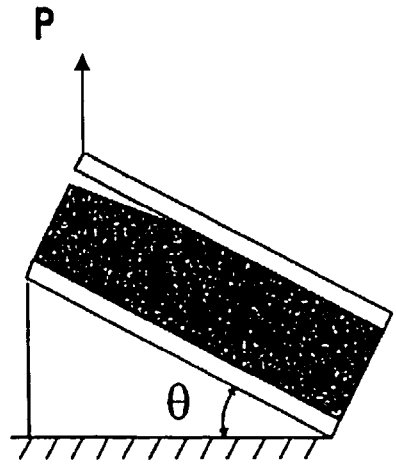
P
θ

Fig. 6

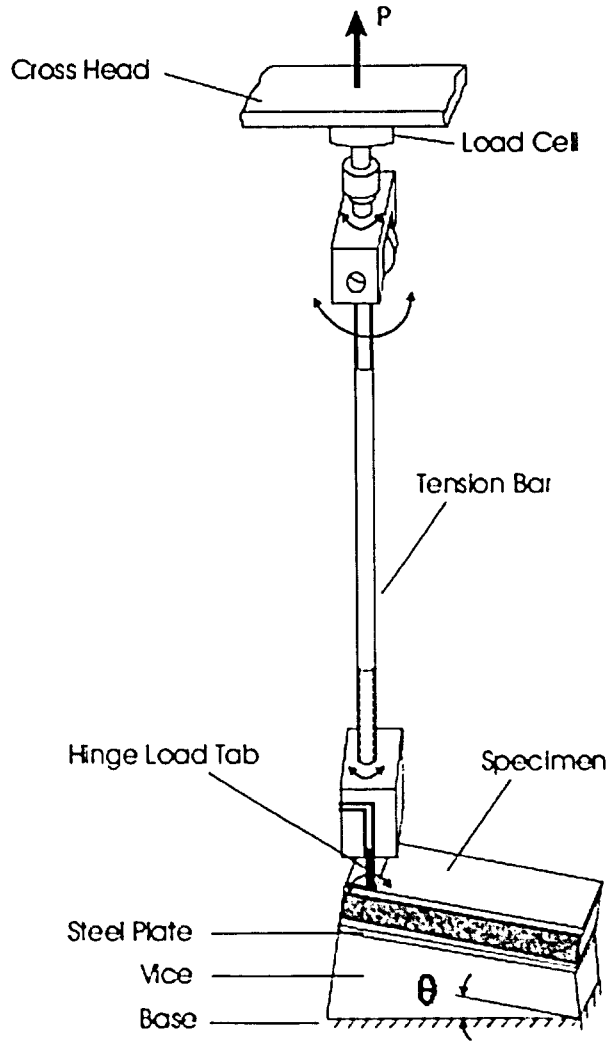
P
Cross Head
Load Cell
Tension Bar
Hinge Load Tab
Specimen
Steel Plate
Vice
Base
θ

Fig. 7

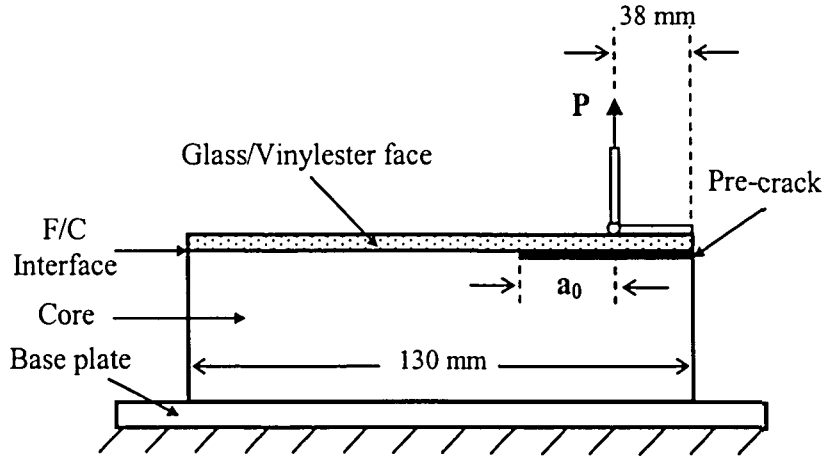
38 mm
P
Glass/Vinylester face
Pre-crack
F/C
Interface
Core
Base plate
$a_0$
130 mm

Fig. 8


66
76
76

(a) (b)

Fig. 9

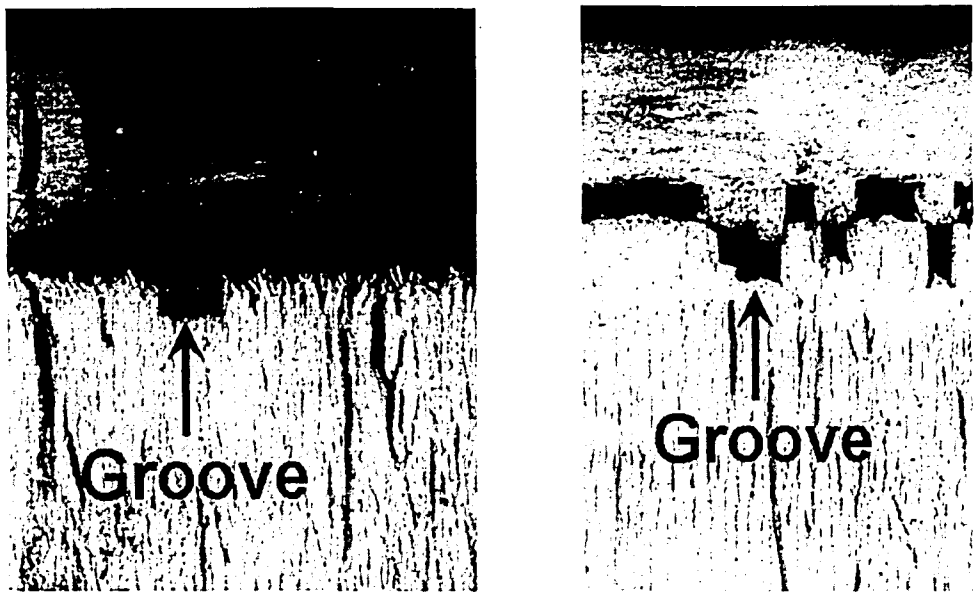


(a) (b)

Fig. 10


(a) (b)

Fig. 11

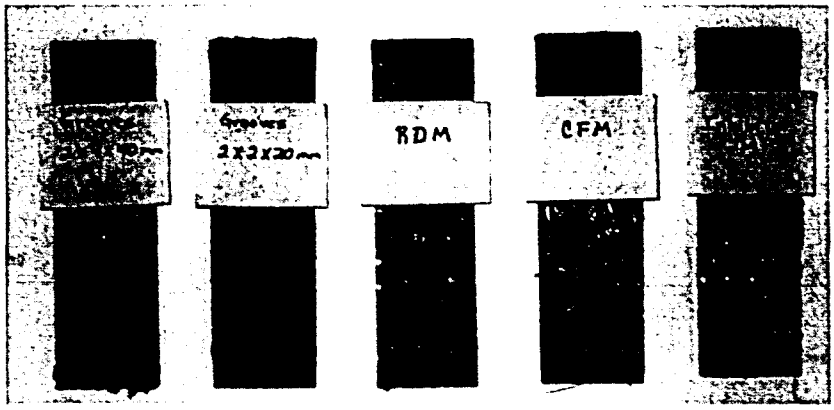


(a)

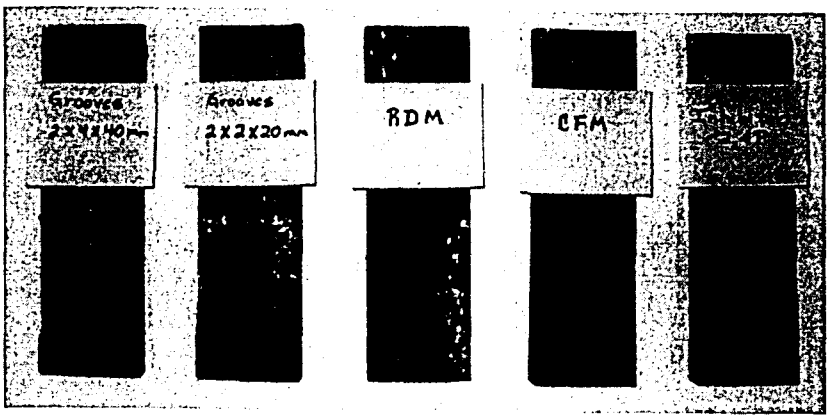
Grooves
2x2x40mm
Grooves
2x2x20mm
RDM
CFM

(b)

Fig. 12

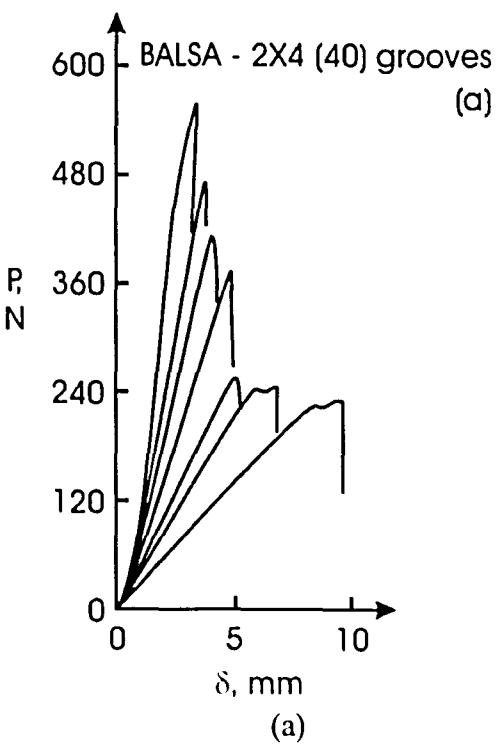
BALSA - 2X4 (40) grooves
(a)
600
480
360
240
120
0
P, N
0
5
10
δ, mm

(a)

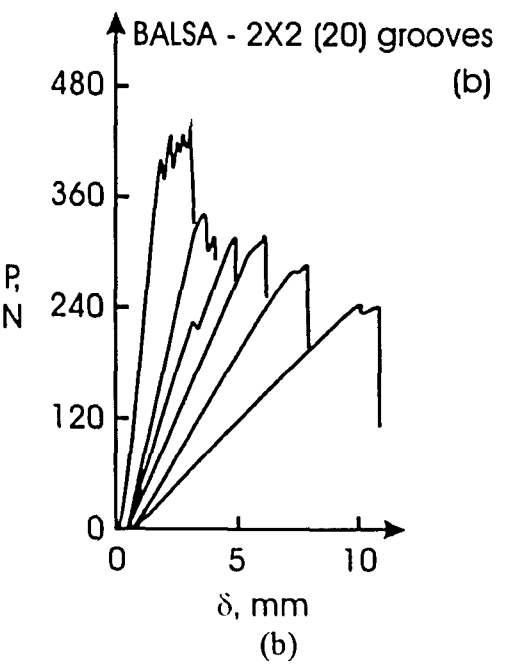
BALSA - 2X2 (20) grooves
(b)
480
360
240
120
0
P, N
0
5
10
δ, mm

(b)

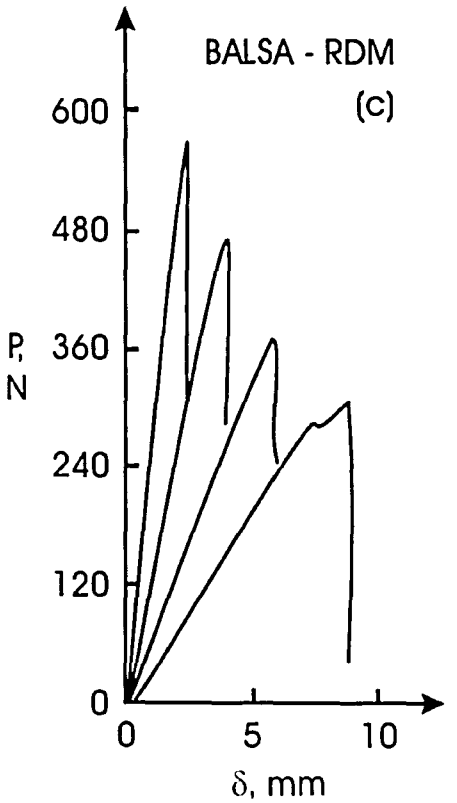
BALSA - RDM
(c)
600
480
360
240
120
0
P, N
0
5
10
δ, mm
(c)

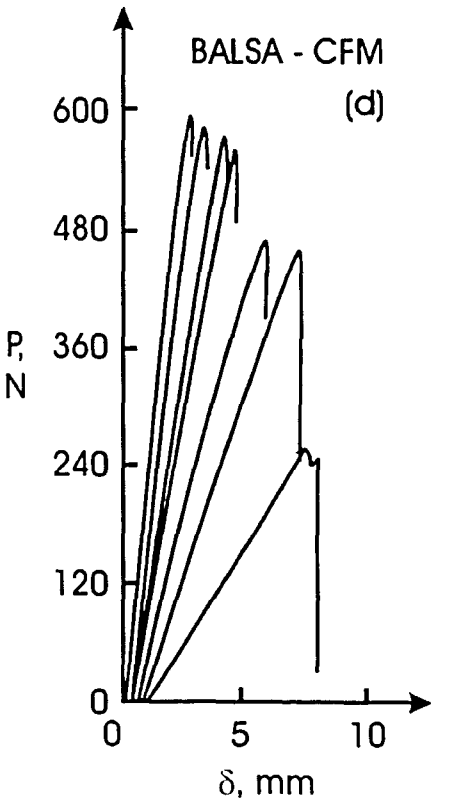
BALSA - CFM
(d)
600
480
360
240
120
0
P, N
0
5
10
δ, mm
(d)

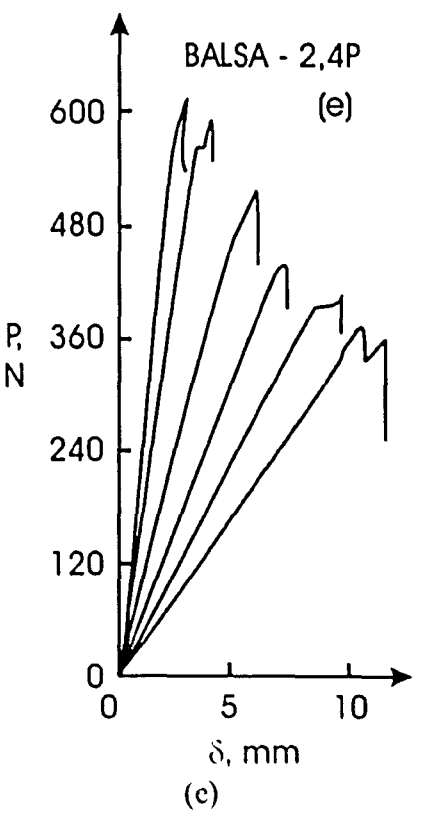
BALSA - 2,4P
(e)
600
480
360
240
120
0
P, N
0
5
10
δ, mm
(e)

Fig.13

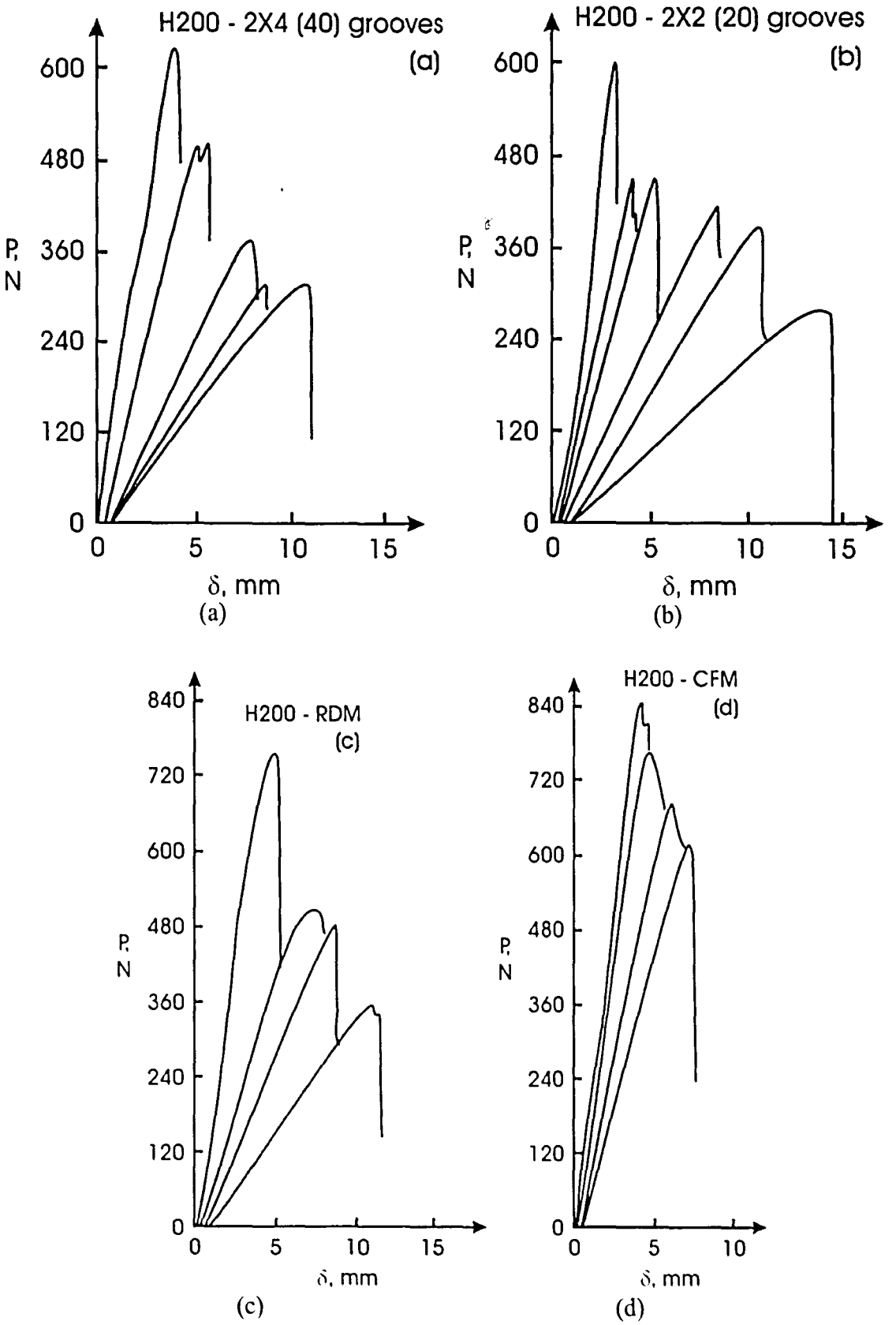
H200 - 2X4 (40) grooves
(a)
600
480
360
240
120
0
P, N
0
5
10
15
δ, mm
(a)
H200 - 2X2 (20) grooves
(b)
600
480
360
240
120
0
P, N
0
5
10
15
δ, mm
(b)
840
720
600
480
360
240
120
0
P, N
H200 - RDM
(c)
0
5
10
15
δ, mm
(c)
H200 - CFM
(d)
840
720
600
480
360
240
120
0
P, N
0
5
10
δ, mm
(d)

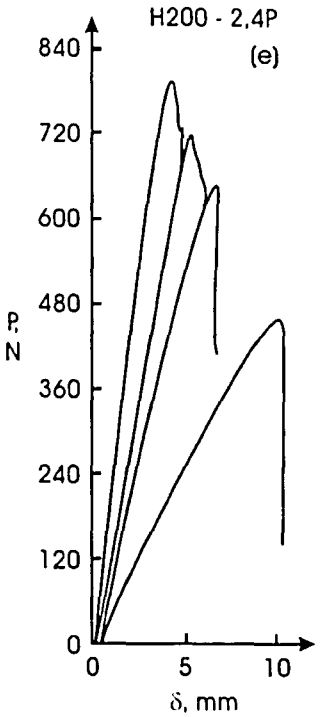

(e)

Fig. 14

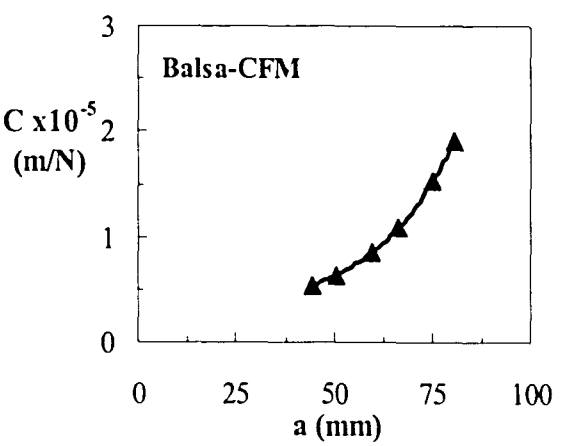


Fig. 15

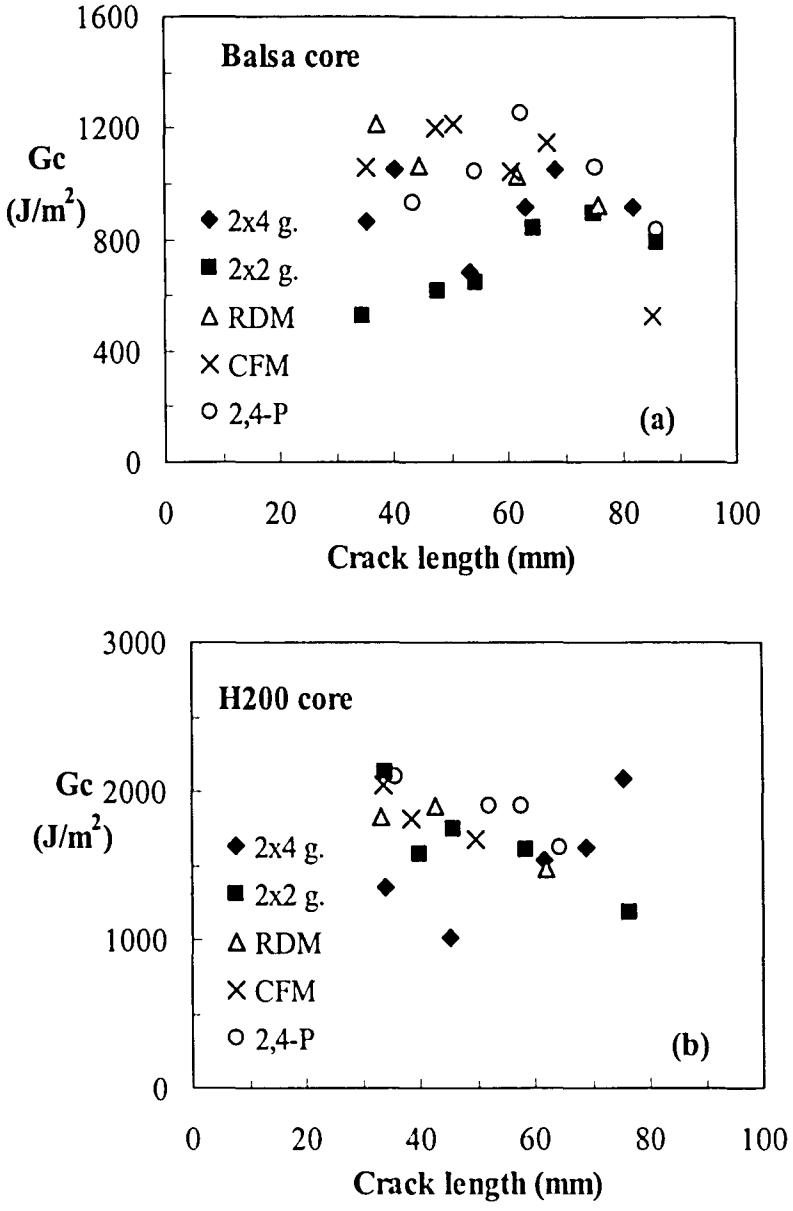
Balsa core
Gc
(J/m²)
1600
1200
800
400
0
2x4 g.
2x2 g.
RDM
CFM
2,4-P
(a)
0
20
40
60
80
100
Crack length (mm)
H200 core
Gc
(J/m²)
3000
2000
1000
0
2x4 g.
2x2 g.
RDM
CFM
2,4-P
(b)
0
20
40
60
80
100
Crack length (mm)

Fig. 16

# Manufacturing and Testing of a Braided Pi Section

Drew Truxel

Joachim L. Grenestedt

Bill Maroun

Lehigh Composites Lab

Dept. of Mechanical Engineering

Lehigh University

19 Memorial Drive West

Bethlehem, PA 18015, USA

Tel. 610-758 4129

E-mail jog5@lehigh.edu

---

**Abstract**

The manufacturing and testing of a three-dimensional braided pi section is described. Tests resulted in a failure load of 3500N and 10500N with the increase caused by surface preparation and curing scheme.

---

## Introduction

Joints often become necessary when assembling several composite sandwich panels. Connections between two structural members represent a zone of potential weakness in the context of composite materials. This is particularly true when the two members are perpendicular to one another. In this case, load is transferred from one member to the other in an out-of-plane mode [1]. In aerospace structures, stiffness and strength to weight ratios, and fatigue and corrosion resistance are extremely important and a lot of research has been done to improve these characteristics. De Jong et al. [2] state that a CFRP plate with a hole will delaminate from the stress concentration if it is overloaded, as opposed to an aluminum plate in which the stress concentration will decrease after an overload due to plasticity. This is one reason fastenerless composite designs are desired. Van Rijn [3] reviews four fastenerless designs for closing a composite wing structure: the Hütter-Hänle method where two L-shaped angles are attached to the sandwich wing skin, and a sandwich web is bonded between the angles; the GROB method where the flanges of a pre-cured I beam are bonded to the wing skins at a location where there is a trough in the skins; the Schleicher method which is similar to the GROB method except for the fact that there is no trough in the wing skins; and the Beechcraft method that uses a 3D braided section bonded to both the skins and the web. Van Rijn [3] considers the latter method a well designed solution capable of taking shear as well as perpendicular loads. Currently, much research is being performed to understand the behavior of three-dimensional braids. Sun and Qiao [4] developed a fiber-inclination model to predict strength based on transverse isotropy of unidirectional lamina and the Tsai-Wu

polynomial failure criterion. They concluded that the braider angle has a significant influence on tensile modulus and strength, and that axial yarns can improve the tensile properties of braided composites. In this paper, a 3D braid is manufactured and tested. One of the applications of this braid is to join composite panels.

**Resin Infusion**

A glass fiber pi shaped braid was received from Bally Ribbon Mills, Fig. 1. The braid was vacuum infused with epoxy to produce a composite pi section. A 0.375" thick aluminum mandrel was manufactured and wrapped with a polymer film to a thickness of approximately 0.400". The braid was placed on a resin distribution medium and wrapped with a peel ply. The aluminum mandrel was inserted between the legs of the pi braid, Fig. 2. A vacuum bag was placed over the assembly and sealed to a flat release agent coated steel plate, Fig. 3. MGS 285 epoxy was mixed with 287 slow hardener, vacuum degassed, and infused by vacuum, Fig. 4. The infusion was made from a bottom edge towards a diagonally opposite top corner. The infusion front was uniform and the infusion produced a part with no dry spots. Demolding presented no problems. Pi section and aluminum mandrel after demolding, Fig. 5.

## Cutting the Pi Section

After demolding, a fixture was made of MDF board to align and clamp the pi section in an abrasive waterjet cutter, Fig. 6. Specimens were made by cutting 1" wide sections, Fig. 7. The cutting produced nice edges with no damage to the composite.

## Bonding the Specimens to the Test Fixture

Two specimens were prepared differently before bonding [5]. The bottom of the first specimen was sanded with 80 grit sand paper while the bottom of the second specimen was grit blasted. Both specimens were cleaned using trichloroethylene. A bonding fixture was developed and manufactured as shown in Fig. 8. The bonding fixture assured that the specimen was centered and true. A specimen is bonded using SIA Adhesives' E2119 A/B in Fig. 9. The specimen and bonding fixture was then placed in an oven for curing the adhesive as well as post curing the epoxy resin of the composite. The curing scheme for the first specimen consisted of a 2°C/min. ramp to 80°C and a soak for an hour, before a slow cool down. The second specimen curing scheme consisted of a 2°C/min. ramp to 76°C and a soak for two hours, before a slow cool down. The assembly was removed from the oven when the temperature had dropped to 50°C. A bonded specimen is shown in Fig. 10.

**Mechanical Testing to Failure**

The specimens were mounted in an MTI modified 10,000 lb screw driven Instron test frame, Fig. 11. The base plate was bolted to the crosshead. The load lug was inserted in mechanical grips, mounted on a universal joint with two unconstrained degrees of freedom. The universal joint was used to reduce the potential of adverse effects due to possible misalignments.

The load and the crosshead displacement were recorded during the tests. The tests were performed under displacement control. The first specimen showed a linear elastic behavior up to a load of 3500 N (790 lb), at which point there was a loud cracking noise and a load drop of approximately 90%, Fig. 12a. The specimen did generate acoustic noise well before the final failure, as is usually the case with composites. After the load drop, there was a hairline crack near the interface between the composite and the steel base plate. This failure location was expected. The displacement was continued and the crack extended outwards in a stable fashion. Post mortem investigation of the crack surface, Fig. 13, showed that the fracture surface was in the fiber/epoxy interface, and not in the adhesive. The pi specimen also had substantial matrix cracking in the corners between the base flange and the legs, as evidenced by white discoloration. The average shear stress between the vertical load lug and the composite legs was on the order of 2.7 MPa (395 psi), which is well below the expected strength of composite as well as adhesive. The average tensile stress under the load lug where the specimen was bonded to

the steel base plate was on the order of 14 MPa (2 ksi), assuming a uniform load over an area with a width of 10 mm (0.4").

The second specimen showed a linear elastic behavior up to a load of 10500 N (2360 lb), at which point there was a loud cracking noise and a load drop of approximately 90%, Fig. 12b. The second specimen failed in a similar fashion to the first, the only difference being a higher critical load. The average shear stress between the vertical load lug and the composite legs was on the order of 8 MPa (1.2 psi), which is well below the expected strength of composite as well as adhesive. The average tensile stress under the load lug where the specimen was bonded to the steel base plate was on the order of 41 MPa (6 ksi). See Table 1 for a summary of results.

**Summary and Conclusions**

Vacuum infusion, waterjet cutting, adhesive bonding and mechanical testing of a pi specimen were performed. The procedures proved successful with no unexpected difficulties. The surface preparation and curing scheme had a significant effect on the failure load. The strength was quite impressive. It may be possible to increase the strength using a different resin and/or changing the fiber architecture under the load lug to locally increase bending stiffness.

**References**

[1]. Junhou, P., Shenoi, R.,'Examination of key aspects defining the performance characteristics of out-of-plane joints in FRP marine structures, Composites Part A, Vol. 27A, pp. 86-103, 1996.

[2]. de Jong, T., Beukers, A., and Vogelsang, L., Weight reduction as an added benefit. In 'Fatigue of Aircraft Materials,' Proceedings of the specialists conference dedicated to the 65$^{th}$ birthday of Professor J. Schijive, Delft University Press, 1992.

[3]. L. P. V. M. van Rijn, 'Towards the fastenerless composite design,' Composites Part A, Vol. 27A, pp. 915-920, 1996.

[4]. Sun, H., Qiao, X., 'Prediction of the mechanical properties of three-dimensionally braided composites,' Composites Science and Technology, Vol. 57, pp. 623-629, 1997.

[5]. Melograna, J. D. and Grenestedt, J.L., "Adhesion of Stainless Steel to Fiber Reinforced Vinyl Ester Composite," Journal of Composites Technology & Research, JCTRER, Vol. 24, No. 4, October 2002, pp. 254-260.

Table 1. Summary of Results

| Specimen # | Bottom surface Preparation | Curing Scheme | | Failure Load (N) | Ave. Shear Stress (Mpa) | Ave. Tensile Stress (Mpa) |
|---|---|---|---|---|---|---|
| | | Temp. (°C) | Time (hrs.) | | | |
| 1 | Sand, clean with trichloroethylene | 80°C | 1 | 3500 | 2.7 | 14 |
| 2 | Grit blast, clean with trichloroethylene | 76°C | 2 | 10500 | 8 | 41 |

**Figure Captions**

Fig. 1 Braid as received.

Fig. 2 Braid covered with peel ply and with aluminum mandrel inserted.

Fig. 3 Braid vacuum bagged and ready for infusion.

Fig. 4 Infusion complete. There were no dry spots.

Fig. 5 Pi section and aluminum mandrel after demolding.

Fig. 6 The pi section is being sliced into 1" wide specimens by a waterjet cutter.

Fig. 7 The 1" wide pi specimens after cutting.

Fig. 8 CAD model of the bonding fixture, which located the specimen in the center of the test base (round green plate) with the load lug indexed in all directions.

Fig. 9 Specimen during bonded.

Fig. 10 Specimen bonded to the base plate and ready for testing.

Fig. 11 Specimen mounted in test frame.

Fig. 12 Load vs. Displacement graphs

a) Specimen 1 b) Specimen 2

Fig. 13 Fracture surface. The crack propagated in the fiber/epoxy interface within the composite (and not in the adhesive).

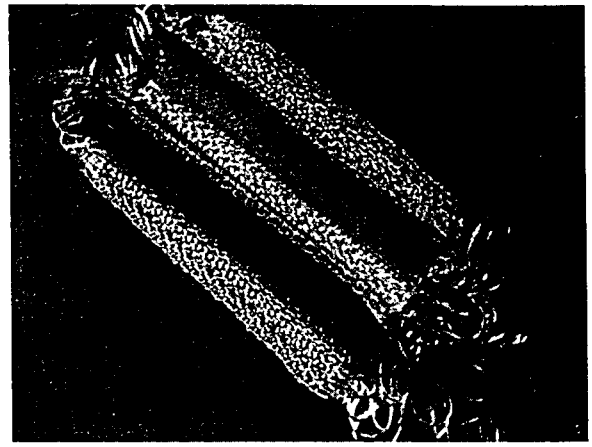

Fig. 1

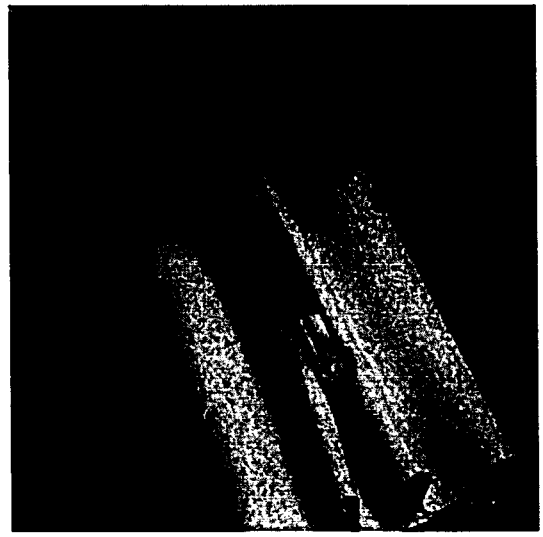

Fig. 2

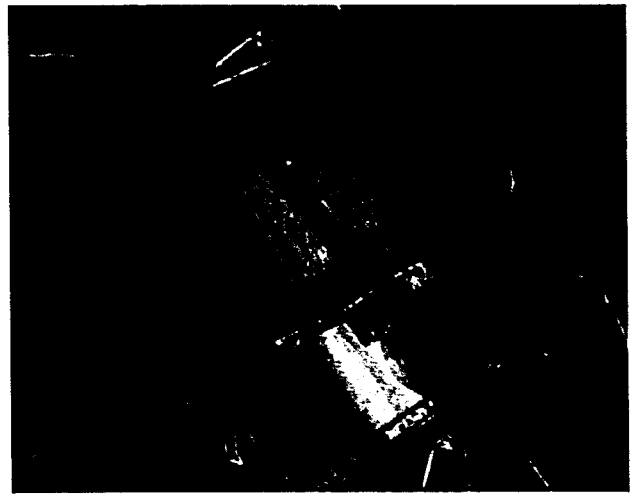

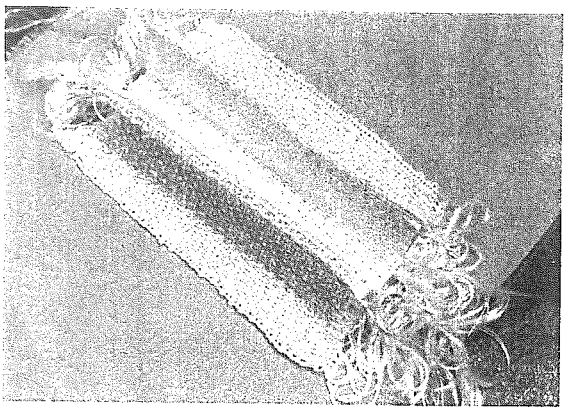

Fig. 1

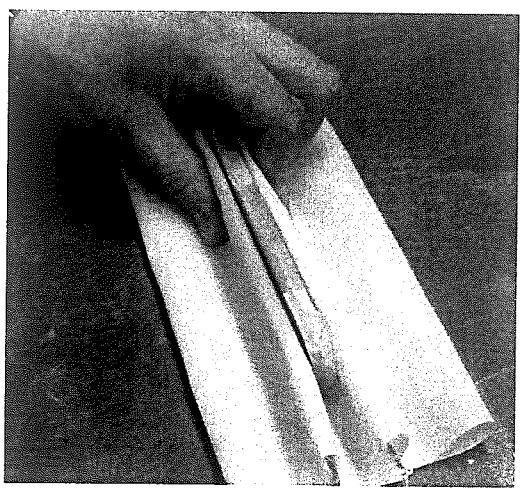

Fig. 2

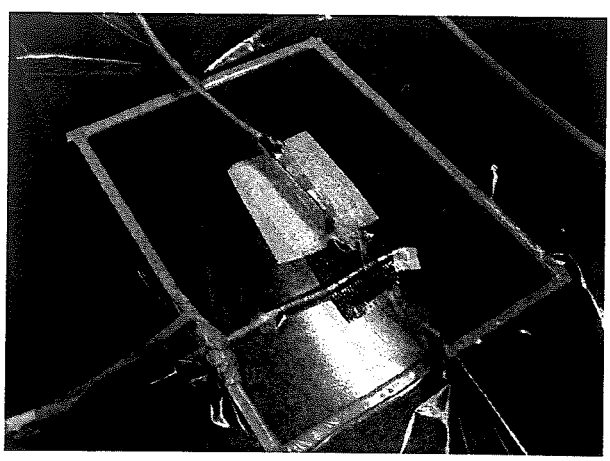

Fig. 3

Fig. 4

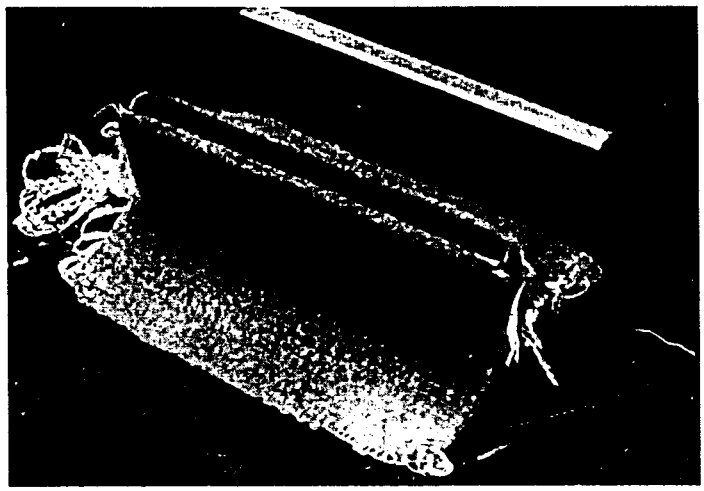

Fig. 5

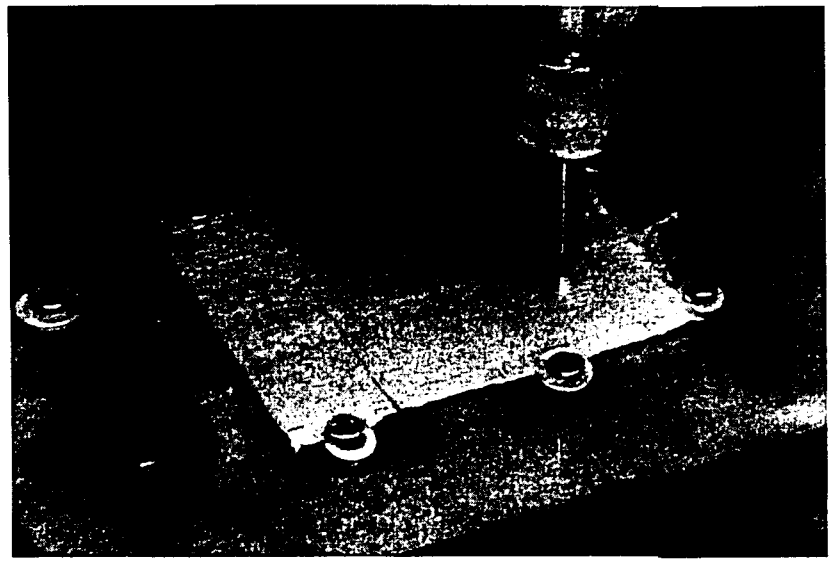

Fig. 6

Fig. 7

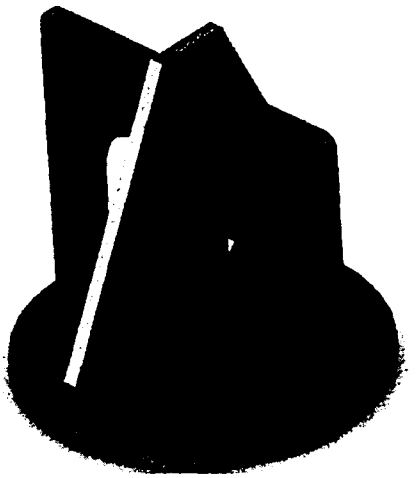

Fig. 8

Fig. 9

Fig. 10

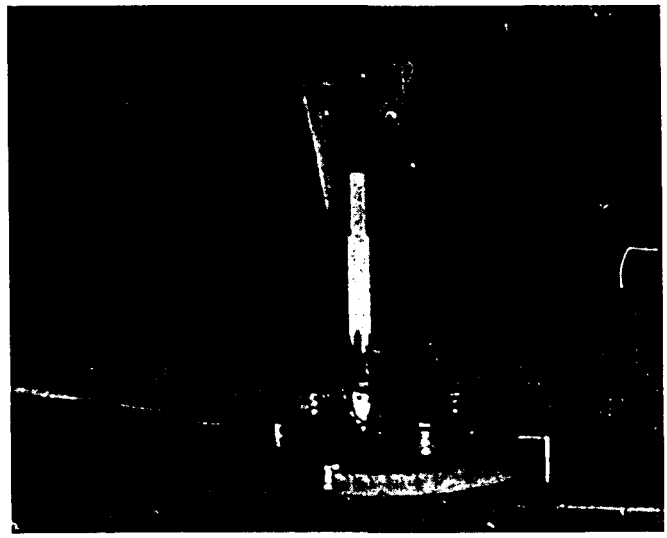

Fig. 11

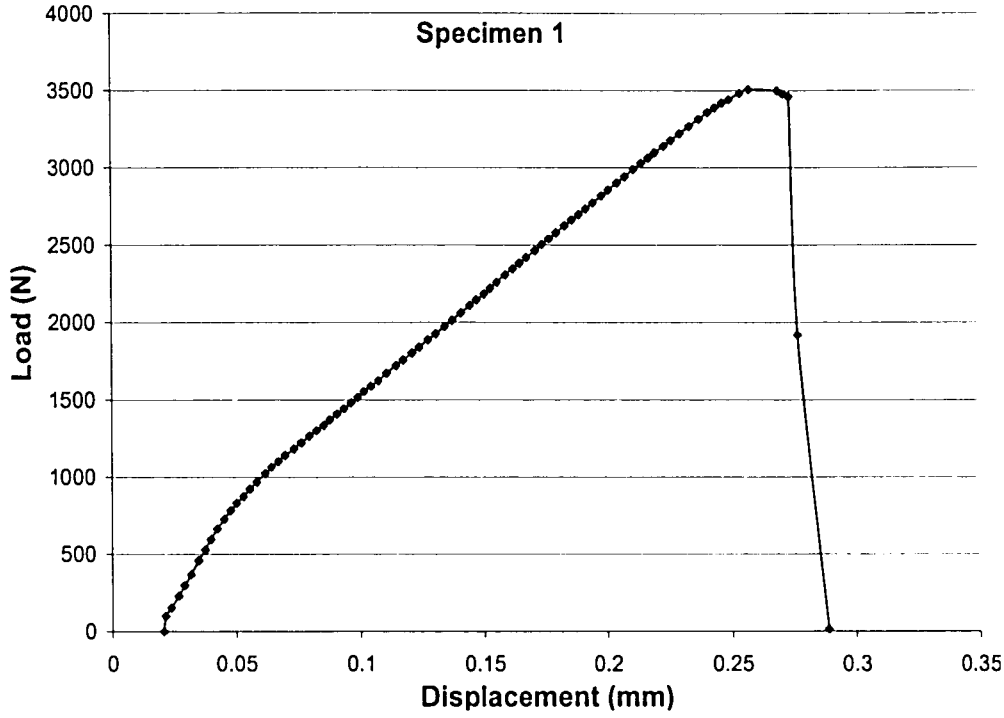
Specimen 1
Load (N)
4000
3500
3000
2500
2000
1500
1000
500
0
0
0.05
0.1
0.15
0.2
0.25
0.3
0.35
Displacement (mm)

(a)

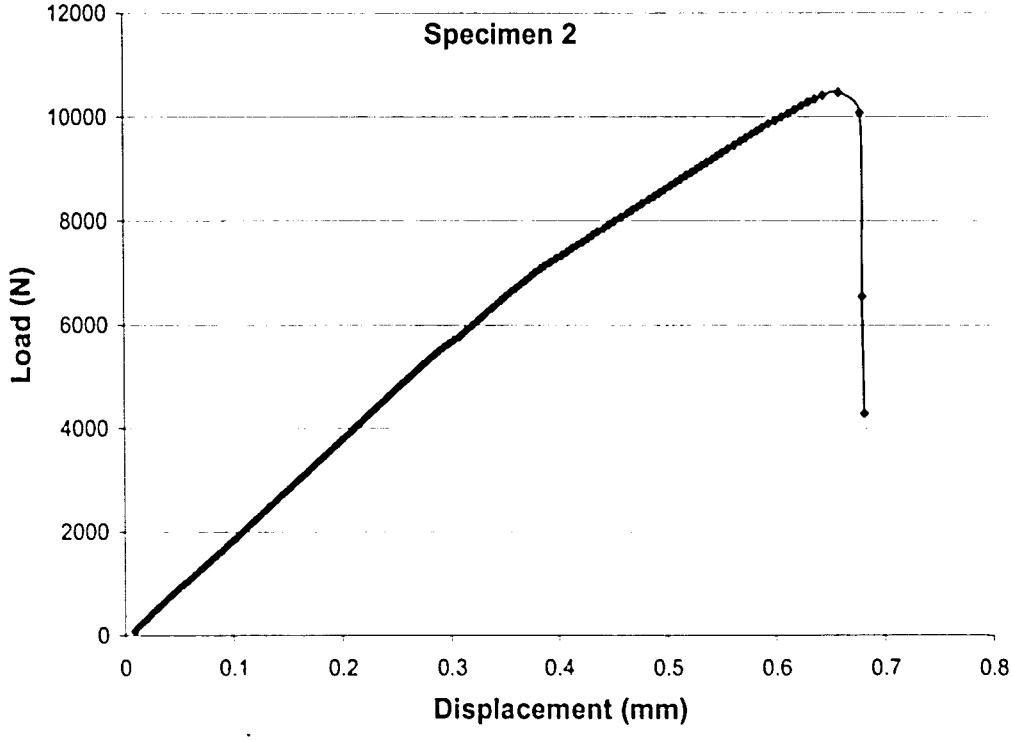
Specimen 2
Load (N)
12000
10000
8000
6000
4000
2000
0
0
0.1
0.2
0.3
0.4
0.5
0.6
0.7
0.8
Displacement (mm)

(b)

Fig. 12

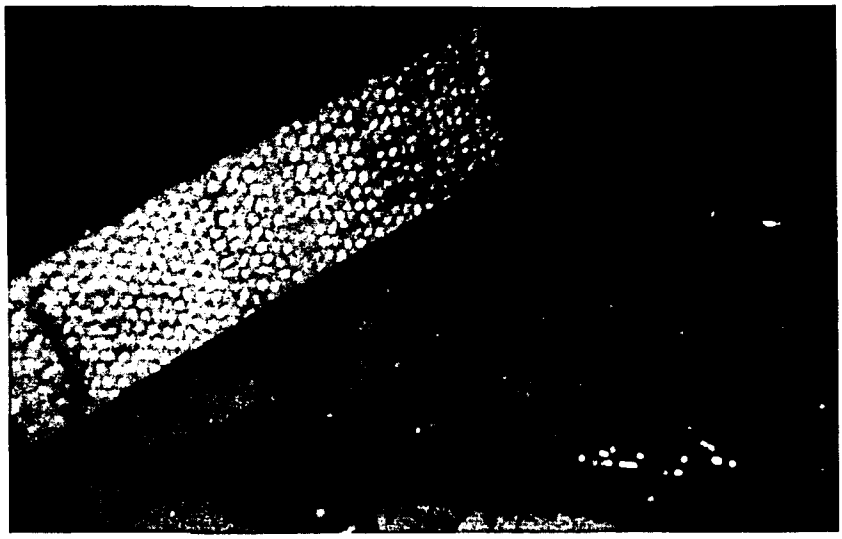

Fig. 13

# Vita

Drew Truxel was born on April 29, 1981 in Summit, New Jersey to his parents, George and Martha. He resided in Warren, NJ where he attended Warren Middle School and Watchung Hills Regional High School. He received 3 varsity letters in football and 4 varsity letters in wrestling. In August of 1999 he began his studies at Lehigh University. During his undergraduate studies he was inducted into Phi Eta Sigma and Pi Tau Sigma honor societies. He graduated May 2003 with a BS in Mechanical Engineering and a minor in Economics. He continued his studies at Lehigh University for his Masters of Science in Mechanical Engineering while working as a research assistant in the Lehigh Composites Lab headed by Dr. Joachim L. Grenestedt. He will be earning his M.Sc. in Mechanical Engineering in May of 2005, after which he will continue with Ph.D. studies at Lehigh University.

# END OF TITLE